Quaternary Science Reviews 305 (2023) 108006

Contents lists available at ScienceDirect

Quaternary Science Reviews

journal homepage: www.elsevier.com/locate/quascirev

New insights into the climate of northern Iberia during the Younger Dryas and Holocene: The Mendukilo multi-speleothem record

J.L. Bernal-Wormull [a, b, *], A. Moreno [a], M. Bartolomé [a], M. Arriolabengoa [c], C. Pérez-Mejías [d], E. Iriarte [e], C. Osácar [b], C. Spötl [f], H. Stoll [g], I. Cacho [h], R.L. Edwards [i], H. Cheng [d, j]

[a] Pyrenean Institute of Ecology - CSIC, 50059, Zaragoza, Spain
[b] Department of Earth Sciences, University of Zaragoza, C/ Pedro Cerbuna 12, 50009, Zaragoza, Spain
[c] Department of Geology, University of the Basque Country, Leioa, Spain
[d] Institute of Global Environmental Change, Xi'an Jiaotong University, 710054, Xi'an, China
[e] Laboratory of Human Evolution-IsoTOPIK Stable Isotope Laboratory, Department of History, Geography & Communication, Edificio de I+D+i, Universidad de Burgos, Pl. Misael Bañuelos s/n, 09001, Burgos, Spain
[f] Institute of Geology, University of Innsbruck, Innrain 52, 6020, Innsbruck, Austria
[g] Department of Earth Sciences, ETH Zürich, 8092, Zürich, Switzerland
[h] GRC Geociències Marines, Dept. Dinàmica de la Terra i de l'Oceà, Facultat de Ciències de la Terra, Universitat de Barcelona, 28080, Barcelona, Spain
[i] University of Minnesota, Minneapolis, MN, 55455, USA
[j] Institute of Earth Environment, Chinese Academy of Sciences, Xi'an, China

ARTICLE INFO

Article history:
Received 7 November 2022
Received in revised form
25 January 2023
Accepted 10 February 2023
Available online 2 March 2023

Handling Editor: Mira Matthews

Keywords:
Holocene
Younger dryas
Iberian Peninsula
Speleothem
North Atlantic
Stable isotopes
Abrupt changes

ABSTRACT

Recent hydroclimate studies on the Iberian Peninsula have shown a complex regional pattern in timing and intensity of climate change spanning the Younger Dryas and the Holocene. These changes are due to multifaceted interactions between climate variability that characterizes the Atlantic Ocean region and hydroclimatic processes associated with the Mediterranean climate, thus making it difficult to reconstruct centennial- and millennial-scale variability in rainfall. In this study we present a composite and continuous isotopic record ($\delta^{13}C$ and $\delta^{18}O$) consisting of four stalagmites from Mendukilo cave (MEN composite) in the western Pyrenees covering the Younger Dryas and the entire Holocene. This record reveals millennial-scale shifts in carbon isotopes in response to changes in the hydroclimate in the northern part of Iberia. The MEN oxygen isotopes show little variation on millenial time scales but reveal centennial changes that correlate with North Atlantic events (e.g., the 8.2 kyr BP cooling event). We observe a delay in the onset of humid conditions in the early Holocene and a subsequent trend towards drier and colder conditions between 6.0 and 2.5 kyr BP. This new, high-resolution and replicated speleothem record denotes the complex connection that exists between the North Atlantic and Western Europe during last millennia and the strong regional heterogeneity of the hydroclimate of Iberia during this time.

1. Introduction

The transition from the cold and dry Younger Dryas to the early Holocene was one of the most rapid warming events on a global scale. This warming was associated with a resumption of the Atlantic Meridional Overturning Circulation (AMOC) (McManus et al., 2004). In the North Atlantic, the onset of the Holocene was punctuated by short cold periods due to variable meltwater input. At latitudes below 45°N, including the Mediterranean region, deglacial warming was influenced by orbitally driven changes (Renssen et al., 2009) that modulated Holocene hydroclimate variability. The general evolution from wetter to drier climatic conditions between the early and late Holocene throughout southern Europe (Roberts et al., 2019) is consistent with the long-term change in insolation, and hence it is influenced by seasonality (Wanner et al., 2008). In fact, the Holocene Mediterranean climate has been traditionally divided into three intervals

* Corresponding author. Pyrenean Institute of Ecology - CSIC, 50059, Zaragoza, Spain.
E-mail address: jluis.wormull@ipe.csic.es (J.L. Bernal-Wormull).

https://doi.org/10.1016/j.quascirev.2023.108006

according to water availability: (1) a first part characterized by humid conditions (11.7–7.0 kyr BP), (2) the mid-Holocene with increased hydroclimatic variability but in general higher temperatures (7.0–5.5 kyr BP), and (3) a decrease in humidity since ~5.5 kyr BP associated with the onset of the current Mediterranean-type climate (Jalut et al., 2009; Magny et al., 2011). In the case of the Iberian Peninsula which is influenced by two contrasting climate regimes (Atlantic and Mediterranean), the hydroclimate evolution during the deglacial warming and the Holocene was characterized by a strong regional heterogeneity (e.g., Carrión et al., 2010). Thus, the observed changes in continental records (lake sediments and speleothems) (e.g., González-Sampériz et al., 2017; Morellón et al., 2018; Moreno et al., 2017) in Iberia are not consistent in space or time with the simplified picture outlined for the Mediterranean region leading to apparent contradictions in temperature and precipitation reconstructions that need to be understood on a regional scale. Different records in the region have highlighted that the sometimes contradictory pattern of climate proxy results may be due to seasonality changes in rainfall (Baldini et al., 2019; Morellón et al., 2009; Moreno et al., 2017; Walczak et al., 2015), potentially due shifts in the position and strength of the Azores High.

Northern Iberia shows large environmental changes along a W-E transect controlled by the altitude and proximity to the ocean, resulting in a large temperature and humidity variability during the Holocene (Finné et al., 2019). For example, the Holocene vegetation and climate succession reconstructed from lakes and peatbogs in NW Iberia and the Eurosiberian region (excluding eastern Iberia) reveals the traditional Holocene regional tripartite pattern (Allen et al., 1996; López-Merino et al., 2012; Moreno et al., 2011): Lake records from the Pyrenees show a progression from a dominantly Atlantic pattern in the western sector (González-Sampériz et al., 2006) to a strong Mediterranean imprint in the central region (Pérez-Sanz et al., 2013). Consistently, lake records present in the central-southern region of the pre-Pyrenees show a delay in the onset of wet conditions (9.5 kyr BP) and a decrease in humidity after 5–4.5 kyr BP (Morellón et al., 2009), a pattern that is supported by terrestrial proxies obtained from western Mediterranean marine records (Fletcher et al., 2013; Frigola et al., 2007). Several Holocene speleothem records have also been obtained from caves in northern Spain, but some are discontinuous (e.g., Serra do Courel; Railsback et al., 2011) or do not cover the entire interglacial (Martín-Chivelet et al., 2011; Rossi et al., 2018). In general, orbital forcing clearly exerted a first-order control on speleothem growth, as shown by an increase in the relative abundance of speleothems (Stoll et al., 2013). Holocene speleothem records also revealed the important role of the Atlantic Ocean in shaping centennial-scale oscillations (Domínguez-Villar et al., 2017; Smith et al., 2016), while a compilation of speleothem records from northern Spain highlighted the role of rainfall seasonality (Baldini et al., 2019).

Here, we present four new stalagmites collected from Mendukilo cave in northern Iberia, which provide a well-replicated, high-resolution and continuous record of northern Iberian climate from the beginning of the Younger Dryas to present-day. Stable isotopes, combined with trace elements and supported by a detailed monitoring of the cave, allow reconstructing temperature and amount of rainfall during last 12,700 years, thus addressing the role of different mechanisms in causing centennial-scale oscillations, such as the 8.2 kyr event. The new data is discussed in both site-specific and regional contexts, together with other published records from the Atlantic margin of Europe, thus offering new insights into the Iberian climate evolution on millennial to centennial time scales since the Younger Dryas.

2. Site description

Mendukilo cave is located at 750 m a.s.l. and 40 km from the Cantabrian coast (Fig. 1A and B) in a site of community importance within the lands of the Astitz council (Larraun valley, Navarra), on the slopes of the eastern part of the Sierra de Aralar (42°58′25″N, 1°53′45″W; Fig. 1B). The cave developed within reef limestones of Lower Cretaceous (Urgonian, Albian-Aptian) age at the eastern boundary of the Basque-Cantabrian basin. The climate of this region is temperate with cool summers (*West coast maritime climate* following the Köppen-Geiger classification). Rain, fog and drizzle are abundant, making this area one of the rainiest locations in Spain (1365 mm of annual precipitation). Rainfall is concentrated in fall, winter and spring, and temperatures are mild, without reaching extremes values, reflecting the proximity of the Atlantic Ocean (Supp. Material Fig. S1). The surroundings of the cave are made up of small karstic mountain plateaus and dolines, with meadows in the highest parts and forests of beech, oak and abundant moss covering the slopes. Soils are well developed, rich in clay, and usually less than 50 cm in thickness.

The cave shows a descending morphology and consists of seven main rooms (Entrance hall, Intermediate gallery, Laminosin gallery, Los Lagos gallery, Dragon hall, Guerrero and Caballo gallery's) (Fig. 1C and D). The total passage length is 869 m and the vertical extension is 59 m (see also Supp. Material).

3. Methods

3.1. Rainfall monitoring

In order to explore the relationship between the isotopic composition of rainfall ($\delta^{18}O_r$ and δD_r) and the climate parameters outside the cave, rainwater was sampled in the University of the Basque Country (Bilbao), an area with a mainly Atlantic source of rainfall and 95 km away from Mendukilo cave (Fig. 1). The sampling was carried out between July 2018 and February 2021 and 144 rain events were sampled. These samples were analyzed for their stable isotopic composition using cavity ring-down spectroscopy (PICARRO L2130-i) at the Pyrenean Institute of Ecology (Zaragoza). The results are reported in per mil with respect to Vienna Standard Mean Ocean Water (V-SMOW) and the reproducibility of the measurements is typically 0.1‰ for $\delta^{18}O$ and 0.5‰–1‰ for δD. The isotopic results were compared to the air temperature measured at the Bilbao airport meteorological station on the day of the respective rain event (Supp. Material Fig. S2).

3.2. Cave monitoring: sampling and analyses

Mendukilo cave was monitored on a seasonal basis for temperature, humidity, pCO_2, dripwater composition and farmed carbonates from 2018 to 2021. Cave-air temperature and relative humidity were recorded using HOBO® U23 pro v2 data loggers in three different galleries (Laminosin, Dragon hall and Guerrero; Fig. 1D). Additionally, pCO_2 was measured using a pSense Portable CO_2 meter (model AZ-0001) at the same sampling points. Precipitation and temperature data obtained from the Aldatz meteorological station, located 5 km northeast of Mendukilo cave (Fig. 1B), were used for comparison.

Dripwater samples were obtained from four different drip sites (MEN-A, MEN-B, MEN-D and MEN-E; Fig. 1D) and, additionally, four pluviometers (RAIN-O-MATIC-HOBO coupled with a HOBO data logger UA-003-64) were used to monitor drip rate (Fig. 1D). All dripwater samples were analyzed for oxygen ($\delta^{18}O_{drip}$) and hydrogen (δD_{drip}) isotope composition via cavity ring-down

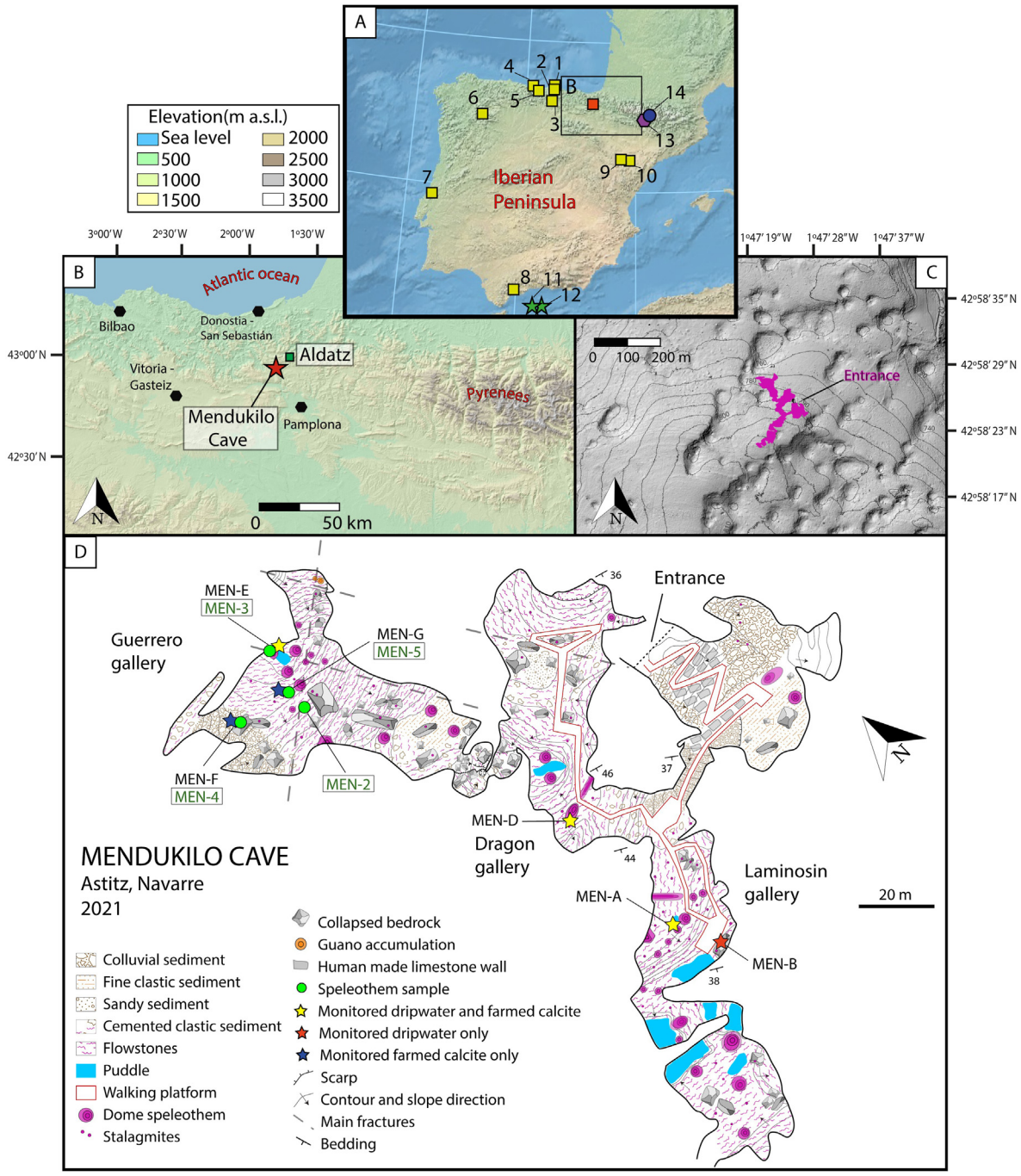

Fig. 1. - A) Location of Mendukilo cave (red square) and other records of the Iberian Peninsula cited in this work (yellow squares = cave sites; green stars = marine records; purple hexagon = lake record; blue circle = ice cave): [1] La Garma Cave; [2] Cueva de Asiul; [3] Kaite Cave; [4] El Pindal Cave; [6] El Soplao Cave; [7] Cova de Arcoia; [8] El Refugio Cave; [9] Ejulve Cave; [10] Molinos cave; [11] ODP976; [12] ALB-2; [13] Basa de la Mora lake; [14] A294 Ice Cave. **B)** Regional setting with the location of the cave (red star), meteorological station (yellow square; where the temperature and rainfall databases for this work were obtained) and nearby major cities (black hexagons). **C)** Digital elevation model and plan view of the cave (pink). **D)** Geomorphological map of Mendukilo cave showing locations of dripwater and speleothem samples.

spectroscopy (PICARRO L2130-i) at the Pyrenean Institute of Ecology (Zaragoza). Results are reported in per mil with respect to Vienna Standard Mean Ocean Water (V-SMOW) and the reproducibility of the measurements is typically 0.1‰ for $\delta^{18}O$ and 0.5‰–1‰ for δD (Fig. 2).

Farmed carbonate precipitated on glass plates (at drip sites MEN-A, MEN-D and MEN-E and additionally at MEN-F and MEN-G sites without drip monitoring) was analyzed for oxygen and carbon isotopes ($\delta^{18}O_{farmed}$ and $\delta^{13}C_{farmed}$, reported as ‰ with respect to the Vienna Pee Dee Belemnite (VPDB) standard). The samples were recovered seasonally. The MEN-E, MEN-F and MEN-G monitoring sites coincide with the locations of the stalagmites examined in this study (MEN-3, MEN-4 and MEN-5 respectively; MEN-2 was not beneath an active drip site). The first batch of isotopic analyses (7 samples) was analyzed at the University of Innsbruck (Austria) using a ThermoFisher Delta V Plus linked to a GasBench II, following the methodology described in Spötl (2011). The long-term reproducibility (1 sigma) of $\delta^{18}O$ is 0.08‰ and 0.06‰ for $\delta^{13}C$ (Spötl,

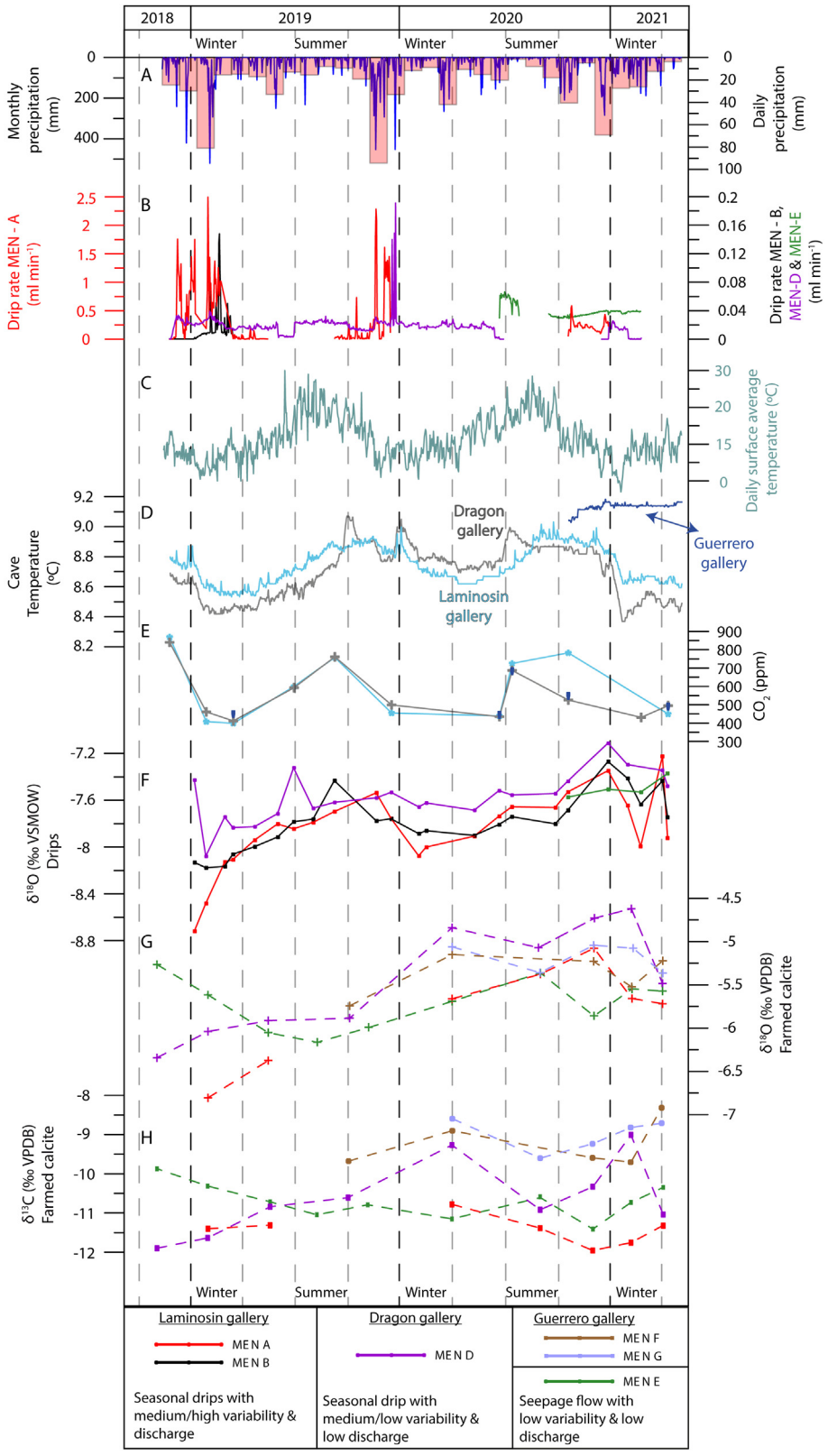

Fig. 2. Monitoring results from Mendukilo cave from November 2018 to May 2021. **A)** Daily and monthly precipitation outside the cave (Aldatz meteorological station). **B)** Drip rate of the different sampling points inside the cave. **C)** Daily surface average temperature outside the cave. **D)** Cave temperature and **E)** CO_2 concentration at the Laminosin (light blue line and dots), Dragon (grey line and dots) and Guerrero (blue line and dots) galleries. **F)** Drip water stable isotope composition of the different drip sites. **G)** $\delta^{18}O$ and **H)** $\delta^{13}C$ values of farmed calcite for the different monitoring sites (see Fig. S3 in the Suppl. for more information).

2011). The rest of the samples were analyzed at the Iso TOPIK Laboratory (University of Burgos; 29 samples) and at the University of Barcelona (10 samples) following similar procedures and identical equipment (Fig. 2).

3.3. Mendukilo stalagmites: petrography, trace elements and stable isotope analyses

Four stalagmites were collected from the Guerrero gallery (Fig. 1D), a deep gallery around 200 m from the cave entrance. Except for MEN-2 these stalagmites were located underneath active drips fed by different fracture networks and dripping conditions (section 4.1). The stalagmites were cut parallel to their growth axis, and the central segment of the slab of each speleothem was sampled for U–Th dating, stable isotopes, and major and trace elements. In MEN-3 and MEN-4, the opposite slab was used to obtain thin sections for a petrographic study (Fig. 3A). MEN-4 is macroscopically very similar to MEN-2 and MEN-5; thus these two last stalagmites were not petrographically analyzed.

A total of 1451 samples for $\delta^{18}O$ and $\delta^{13}C$ analysis were obtained along the central axis at 1 mm increments from stalagmites MEN-2, MEN-3, MEN-4 and MEN-5. Isotopic analyses were performed at the University of Innsbruck, using a ThermoFisher Delta V Plus linked to a GasBench II, following the methodology described in Spötl (2011). The long-term reproducibility (1 sigma) of the $\delta^{18}O$ analyses is 0.08‰ and 0.06‰ for $\delta^{13}C$ (Spötl, 2011). All values are reported as per mil with respect to the Vienna Pee Dee Belemnite standard (VPDB).

In addition to the isotope samples, 267 carbonate samples were analyzed for trace elements. Samples were taken at 5 mm intervals and measured for Mg/Ca and Sr/Ca ratios at ETH Zurich (Agilent QQQ 8800) using a standardization approach similar to that reported in Stoll et al. (2022).

3.4. U–Th dating and age model development: integration into a composite record

A total of 41 powder samples were drilled for uranium-series dating from distinct growth layers along the central growth axis of each speleothem using a handheld drill and a tungsten carbide drill bit. After chemical separation, U and Th isotope measurements were performed using a MC-ICP-MS (Thermo-Finnigan Neptune Plus) at the University of Xi'an and the University of Minnesota (USA), following a previously described methodology (Cheng et al., 2013). To calculate corrected ages an initial $^{230}Th/^{232}Th$ atomic ratio of $4.4 \pm 2.2 \times 10^{-6}$ was used.

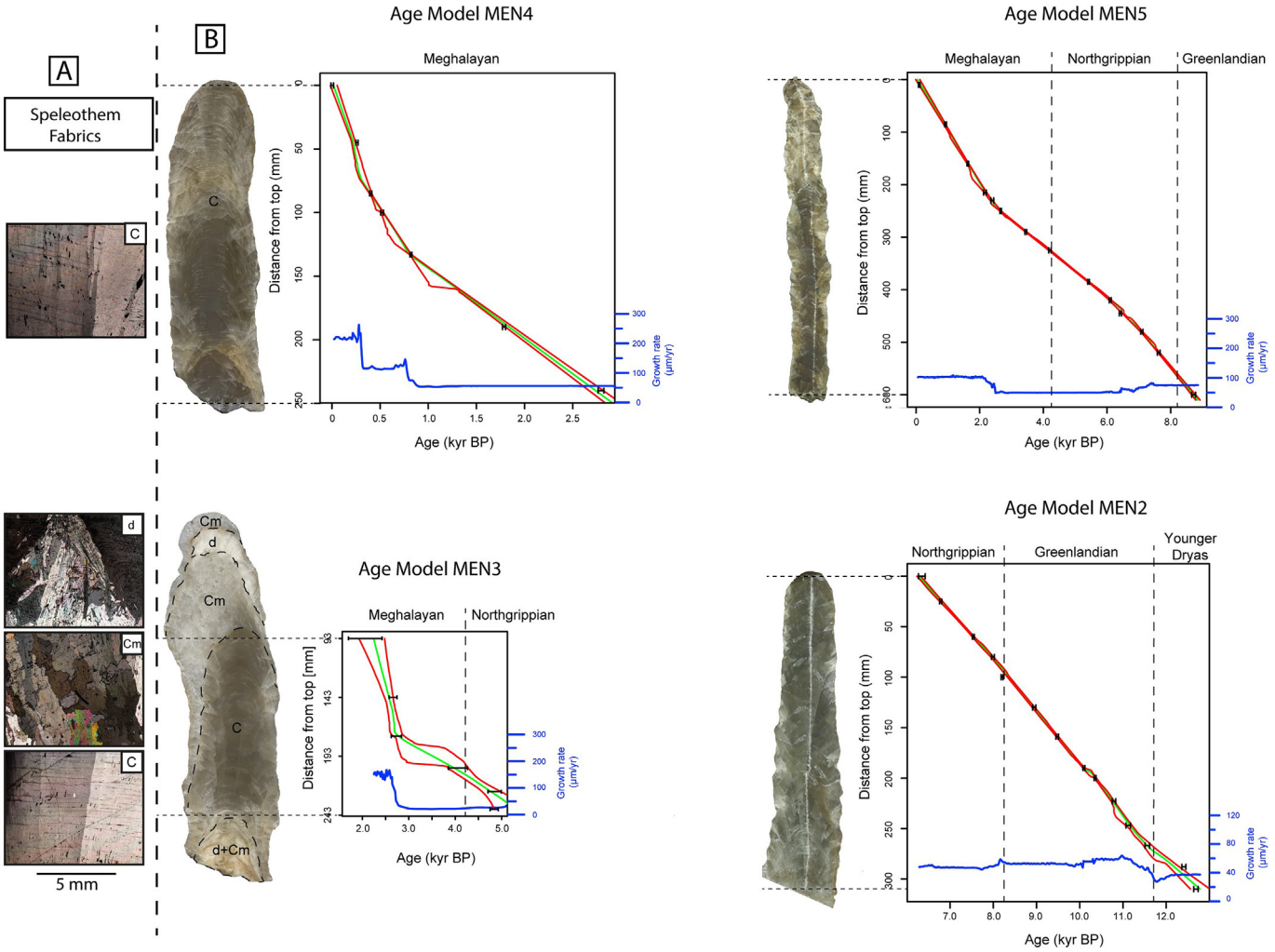

Fig. 3. A) Thin sections showing the main fabrics of stalagmites MEN 4 (columnar fabric [C]) and MEN 3 (transition between columnar, columnar microcrystalline [Cm] and dendritic [d] fabrics). **B)** Dating results (black dots with error bars) and age models of the four stalagmites (green line) with their corresponding error limits (red lines) as obtained using StalAge. Changes in growth rate (blue line) are also indicated.

The individual age model for each stalagmite has been obtained using the software *StalAge* (Scholz and Hoffmann, 2011) (Fig. 3B). Later, the individual isotope profiles of the four stalagmites were integrated into a single one (MEN composite record) using the software *Iscam* (Fohlmeister, 2012). This program looks for the highest correlation between two or more dated proxy signals within age uncertainties using a linear interpolation between adjacent U–Th dates. Two composite records have been constructed by applying the $\delta^{13}C$ and then the $\delta^{18}O$ data from the different stalagmites of the Mendukilo cave. The isotopic values between the different stalagmites in the overlapping intervals correlate well with each other in each of the composites ($\delta^{13}C$ and $\delta^{18}O$), but finally it has been decided to use the $\delta^{13}C$ composite (and the resulting age model) throughout this work, since it presents a greater variability in its isotopic values over the last 13 kyr BP. Finally, the age model that produced the highest coherence (applying a smoothing of 100 years) was selected and subsequently the data from other proxies of this work ($\delta^{18}O$ and trace elements) have been assigned a chronology based on this new $\delta^{13}C$ composite age model.

4. Results

4.1. Monitoring

The average annual rainfall in the area (1921–2021) is 1365 mm (Supp. Material Fig. S1). Rainfall amount during the monitored years shows an important interannual variability, with a decreasing annual amount from 2019 (1931 mm) to 2020 (1371 mm) (Fig. 2A). Drip data (November 2018 to May 2021) reveal that the MEN-D and MEN-E drip sites were continuously dripping. They show a lower drip-rate variability between different seasons compared to the MEN-A and MEN-B drip sites, which tend to almost cease in summer (Fig. 2B). Episodes of highest drip rates per day recorded by the MEN-A and MEN-B loggers correlate with periods of intense daily (>50 L/m^2) and monthly rainfall (winter and fall in 2019, Fig. 2A). Drip sites MEN-A, MEN-B and MEN-D are fed by low discharge seasonal drips with a medium to high variability, with a maximum discharge rate of 2.49 ml min^{-1}, 0.15 ml min^{-1} and 0.17 ml min^{-1} and a coefficient of variation of 134, 90 and 59, respectively (following Smart and Friederich (1987), Supp. Material Fig. S3). On the other hand, MEN-E is fed by seepage flow (low variability, coefficient of variation of 21) showing the lowest maximum discharge rate of 0.06 ml min^{-1}. In the case of drips without drip rate monitoring (MEN-F and MEN-G) they have been categorized as continuous drips (not seasonal) in the different monitoring campaigns inside the cave and with an apparent similar behavior between MEN-E and MEN-D drips. The classification of drips based on discharge rate and coefficient of variation has been shown to be useful to discern its influence on the isotopic composition of the dripwater and of the farmed calcite (Pérez-Mejías et al., 2018).

The air temperature inside Mendukilo cave varies between 8.4 and 9.2 °C during the year, i.e. 3.4 °C lower than the mean annual surface air temperature in the monitored years (11.8–12.6 °C, Aldatz meteorological station) showing a delay of about 10–14 days in relation to variations in surface temperature (Fig. 2C and D). Only the temperature sensor installed in the Guerrero room, far from the entrance, recorded a constant temperature (9.1–9.2 °C). pCO_2 values follow the seasonal temperature pattern inside the cave, being higher in summer and lower in winter.

For the studied period, $\delta^{18}O_{drips}$ and δD_{drips} values for the four drip sites range from −8.7 to −7.3‰ and −53.8 to −42.0‰, respectively. The mean $\delta^{18}O_{drips}$ values for these drip sites are between −7.6‰ (MEN-D and MEN-E) and −8.0‰ (MEN-A and MEN-B) and, in general, winter values are lower than summer values (Fig. 2F). Considering the average values for all drip sites during summer (−7.6‰) and winter (−8.1‰), the average seasonal variability is 0.5‰. Adding to this variability, a slight trend towards less negative values is observed between 2018 and 2021 associated with a decreasing amount of rainfall as described above. The exception is the MEN-E drip site which fed the MEN-3 stalagmite and records a stable drip rate that does not respond to seasons or rain events and shows a low isotopic variability (Fig. 2). The seasonality recorded in the dripwaters (low variability) values was also observed in rainfall (high variability; Fig. S2), although it was much more reduced in the first one due to homogenization once water enters into the epikarst.

Carbonate precipitated on glass slides all year round and the $\delta^{18}O_{farmed}$ and $\delta^{13}C_{farmed}$ values range from −6.8‰ to −4.6‰ and from −12.0‰ to −8.3‰, respectively (five different sampling points, Fig. 2G and H). Except for drips MEN-E, MEN-F and MEN-G, farmed calcite results show a tendency towards less negative values (statistically significant for $\delta^{18}O_{farmed}$) during the second half of 2020 and the first part of 2021 (mean $\delta^{18}O_{farmed}$ −5.3‰) compared to the period 2018–2020 (mean $\delta^{18}O_{farmed}$ −6.3‰; Fig. 2G). Comparing $\delta^{18}O_{drip}$ with $\delta^{18}O_{farmed}$ of each drip site shows that calcite precipitated close to isotopic equilibrium. The amount of rainfall is thus likely influencing $\delta^{18}O_{farmed}$ on an interannual scale but the seasonal impact is less pronounced. This seems to be true for $\delta^{13}C_{farmed}$ as well, although the MEN-D drip site shows seasonal variability in the 2020–2021 time interval where the highest $\delta^{13}C_{farmed}$ values coincide with low pCO_2, thus suggesting enhanced degassing and possible prior calcite precipitation (PCP). An interesting feature is that $\delta^{13}C_{farmed}$ shows less negative values for the seepage drip and nearby drips of the same cave gallery (MEN-F and MEN-G) in comparison to faster drips (Fig. 2H).

4.2. Petrography, chronology and stable isotopes of the Mendukilo stalagmites

Stalagmites MEN-2 (31.0 cm), MEN-4 (25.6 cm) and MEN-5 (61.0 cm) consist of coarsely crystalline calcite and are macroscopically homogeneous without any signal of recrystallization. They are made of columnar fabric, lack growth hiati and do not show macroscopically visible laminae (Fig. 3A). Stalagmite MEN-3 (28.0 cm) is an exception showing a more porous, columnar microcrystalline fabric passing into a dendritic type at the base (the first 4.0 cm) as well as close to the top (between 18.5 and 28.0 cm from the base - Fig. 3A). According to Frisia (2015), this transition suggests a change from a relatively slow and constant discharge to more variable drip rates.

U–Th dating revealed that these four stalagmites grew continuously over different intervals of the Holocene and Younger Dryas (YD). Taking together, they cover continuously the entire Holocene and the YD (i.e., since 12.8 kyr BP) with a good overlap (Fig. 3): MEN-2 grew between 12.8 and 6.3 kyr BP, MEN-3 between 6.0 and 0 kyr BP, MEN-4 covers the last 3.0 kyr, and MEN-5 spans the last 8.8 kyr. The dating of the base and top parts of stalagmite MEN-3 was challenging given the change in petrography (see above; Supp. Material Table S1). Measured U concentrations in Mendukilo stalagmites range between 73 and 350 ppb, and the measured $^{230}Th/^{232}Th$ activity ratio varies between 20 and 9500. Each of the MEN stalagmite age models have fairly low uncertainty of the corrected ages ranging between 0.005 and 0.250 kyr BP (the average error of the MEN-2, MEN-4 and MEN-5 age models are 0.055, 0.041 and 0.040 kyr BP respectively). In the case of MEN-3 the errors are larger fluctuating between 0.060 and 0.800 kyr BP (average error of 0.212 kyr BP). Average growth rates of MEN-3 (145 μm/yr) and MEN-4 (224 μm/yr) are higher than for MEN-2 (68 μm/yr) and MEN-5 (77 μm/yr), indicating higher speleothem

growth rates during the late Holocene in this cave compared to the YD and early Holocene (Fig. 3).

The $\delta^{18}O$ and $\delta^{13}C$ values of the four stalagmites range from −6.3 to −4.3‰ and from −10.4 to −4.4‰, respectively, with similar amplitudes in the overlapping intervals (Suppl. Material Fig. S4 and Fig. S5). This replication supports the use of these isotopic profiles as reliable proxy records. The only exception is the upper part of stalagmite MEN-3 which differs markedly from MEN-4 and MEN-5 in its stable isotope values (Suppl. Material Fig. S4 and Fig. S5). Given the fact that this part of MEN-3 also shows a different type of calcite fabric we excluded this part.

4.3. Composite record from Mendukilo cave

The MEN composite generated with *Iscam* for both $\delta^{13}C$ and $\delta^{18}O$ isotopic records covers the last 12.7 kyr BP with an average growth rate of 130 μm/yr. The $\delta^{13}C$ composite record shows values between −9.5 and −4.5‰ ($MEN_{\delta 13C\ mean} = -6.6‰$; $MEN_{\delta 13C\ STD} = 0.8‰$; Fig. 4). In the case of $\delta^{18}O$ the values are characterized by a lower amplitude and variability, ranging from −6.3 to −4.3‰ ($MEN_{\delta 18O\ mean} = -5.4‰$; $MEN_{\delta 18O\ STD} = 0.3‰$; Fig. 4). For the composite we included the stalagmites from the youngest to the oldest one to maximize the correlation coefficient. The $\delta^{13}C$ correlation between MEN-3 and MEN-4 is high (r = 0.97) but they only intersect at a gap of about 0.5 kyr; when adding MEN-5 the correlation decreases (r = 0.37) reflecting bad interrelation in the overlapping intervals of stalagmites MEN-5, MEN-4 and MEN-3 during the last 3 kyr (Suppl. Material Fig. S4 and Fig. S5). Thus, paleoclimatic interpretations for the last 3 kyr should be viewed with caution. Finally, when combining this composite with the MEN-2 record, the final correlation is very high (r = 0.91). The MEN composite data contains results from mathematical interpolation, therefore, abrupt variations in the MEN composite should be treated and interpreted with caution and always taking into account the isotopic (Fig. S4 and Fig. S5) and trace element (Fig. S6 and Fig. S7) records of each stalagmite separately.

The composite record produced by *Iscam* shows that the YD starts with opposite trends when comparing both isotopic records (Fig. 4). The $\delta^{13}C$ values increase (from −6.7 to −5.6‰) and those of $\delta^{18}O$ decrease (from −4.6 to −5.2‰) at the onset of the YD. The values remain stable during the YD, and at its end the $\delta^{13}C$ values gradually decrease (from −5.6 to −7.8‰) while the $\delta^{18}O$ values increase abruptly (from −5.2‰ in the YD to −4.3‰ at 11.6 kyr BP) reaching the highest values of the entire record at the YD-Holocene transition (Fig. 4).

MEN composite $\delta^{13}C$ data show a significant trend towards more negative values during the first part of the Greenlandian, from −6.0‰ at 11.7 kyr BP to −8.1‰ at 10 kyr BP (Fig. 4). Afterwards, the values remain stable, only interrupted by a short interval of higher values between 9.3 and 9.1 kyr BP. The highest $\delta^{18}O$ values of the composite are present in the early Greenlandian and show a trend towards lower values (as the $\delta^{13}C$ record) but lasting until the end of the Greenlandian (from −5.0‰ at 11.68 kyr BP to −5.7‰ at 8.23 kyr BP). During the Northgrippian (8.2–4.2 kyr BP) the $\delta^{13}C$ record shows a progressive trend towards higher values: from −8.0‰ at 7.9 kyr BP to −4.8‰ at 4.1 kyr BP (Fig. 4). During the first part of the Northgrippian (8.2–6.5 kyr BP) the $\delta^{18}O$ values are very negative and increase in the second part (mean 5.2‰ between 6.5 and 4.2 kyr BP). The lowest $\delta^{18}O$ values of the MEN composite record are present by extreme values of −6.3‰ at 7.0 and 8.1 kyr BP. The $\delta^{18}O$ variability during the Meghalayan (4.2 kyr BP to present) is small and lacks a trend. $\delta^{13}C$ values show the highest values from

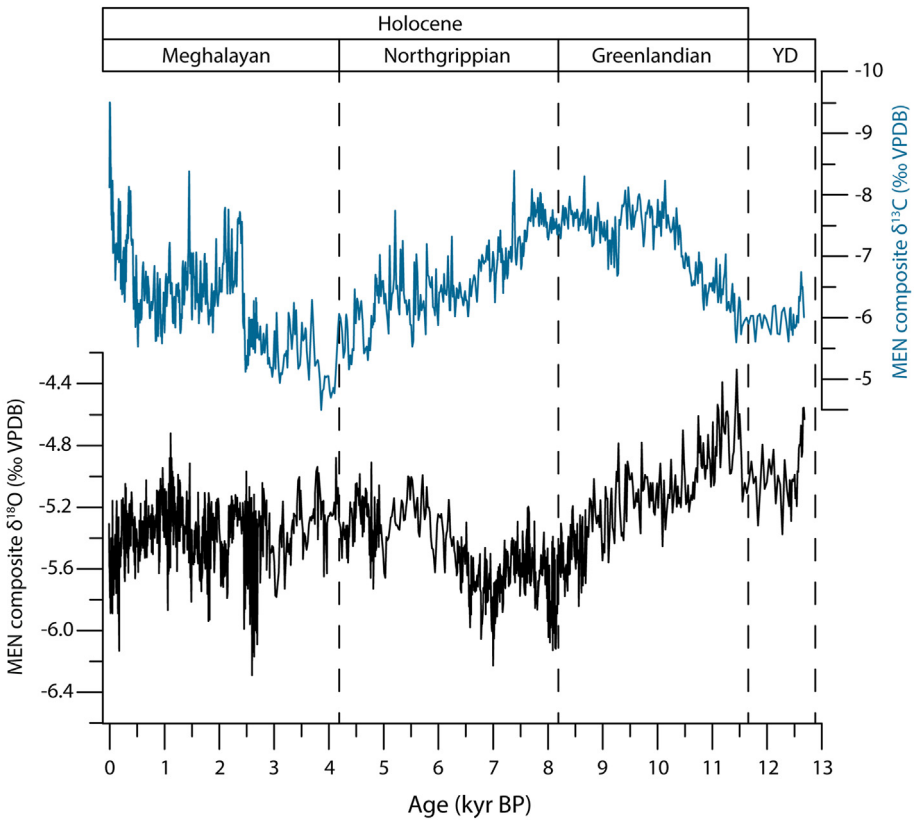

Fig. 4. Mendukilo isotope composites for $\delta^{13}C$ (upper panel; note inverted y-axis) and $\delta^{18}O$ (lower panel) for the last 13 kyr obtained using Iscam combining four stalagmites. The Holocene division follows Walker et al. (2019).

4.2 to 2.5 kyr BP, but by comparing the $\delta^{13}C$ values of the composite with those of stalagmites MEN-3 and MEN-5 it is possible to detect that there is a distortion in the former during the time interval of 4.2 and 3.5 kyr BP. This over-exaggeration of the $\delta^{13}C$ data in the composite is clearly an artifact of the mathematical algorithm, so that interpretations at millennial and centennial scales during that time interval must take into consideration the $\delta^{13}C$ values shown by stalagmites MEN-3 and MEN-5 separately from the composite. The MEN $\delta^{13}C$ composite shows a rapid shift towards lower isotope values at 2.5 kyr BP (Fig. 4).

Mg/Ca ranges between 0.40 and 1.60 mmol/mol (Suppl. Material Fig. S6) and shows greater variations in trends among the four stalagmites. Sr/Ca measured in the four stalagmites show similar temporal patterns and are spanning the same range of values (0.12–0.06 mmol/mol) (Suppl. Material Fig. S7). Sr/Ca values are low during the YD and increase during the Greenlandian, reaching high values around 10 kyr BP. This is followed by a decreasing trend until 3.5 kyr BP and an increasing trend until modern conditions. Sr/Ca is anticorrelated with $\delta^{13}C$ at the millennial time scale (correlation coefficient -0.37, $n = 1288$, $p \ll 0.01$) (Suppl. Material Fig. S8). The Ba/Ca ratio of the MEN composite shows strong similarities with Sr/Ca, but correlation among the four stalagmites is less good, so we only use Sr/Ca to compare with other proxies. In particular, the trends during the last 3000 years are not well replicated among the four speleothems and thus not considered for discerning the climate signal. We also assess the potential effect of in-cave processes such as PCP on the $\delta^{13}C$ record looking for the most robust proxy trends associated to more constant Mg/Ca ratios of the MEN-5 stalagmite (Suppl. Material Fig. S9).

5. Discussion

5.1. Controls on MEN geochemical proxy data

Trace elements in speleothems are useful paleoclimate indicators in caves where seasonal and long-term changes in water balance result in large and systematic change in Mg/Ca, Sr/Ca and Ba/Ca in dripwater associated with PCP during the dry season (Fairchild and Treble, 2009). In Mendukilo stalagmites, Mg/Ca and Sr/Ca show a contrasting pattern (Suppl. Material Fig. S6 and Fig. S7), indicating that PCP cannot be the dominant control on both ratios. One explanation could be a significant non-bedrock source of Mg or Sr which varied temporally. In caves very close to the coast, such as Pindal Cave with galleries 200 m from the sea cliff, marine aerosols can be a significant source of Mg in the Holocene (Moreno et al., 2010). However, in the cave of Mendukilo, 50 km from the Atlantic coast and at 750 m elevation, surrounded by mountain ranges of higher altitude, a dominant marine aerosol contribution of Mg is not expected, and temporal changes in Mg/Ca are unlikely to reflect changes in marine aerosol Mg delivery. An alternative explanation for the differences in Mg and Sr could be decoupled temporal changes in the partitioning coefficient of either Sr or Mg. Many studies have documented variations in the Sr partitioning coefficient driven by calcite growth rate (Lorens, 1981; Nielsen et al., 2013; Tan et al., 2014; Tang et al., 2008; Tesoriero and Pankow, 1996), and this is a common explanation for the decoupling of Mg/Ca and Sr/Ca in stalagmites (Stoll et al., 2012; Warken et al., 2018). We observe that Sr/Ca in Mendukilo stalagmites positively correlates with growth rate (correlation coefficient $= 0.55$, $n = 1288$, $p \ll 0.01$) deduced from the U–Th age models (Suppl. Material Fig. S10), suggesting that growth rate contributed to the Sr/Ca variations. Consequently, we infer that Sr/Ca may be driven by the growth rate effect superimposed on PCP, whereas Mg/Ca may reflect temporal variations in PCP. In fact, Sr/Mg of stalagmites allows isolating the correlation between Sr/Ca and growth rate (Suppl. Material Fig. S8). Since stalagmites fed by different drip routes may have different sensitivities to PCP, Mg/Ca of coeval stalagmites may not covary as is the case in this work. On the contrary, the existence of common drivers of dripwater saturation by soil pCO_2 may lead to more reproducible variations in growth rate and Sr/Ca.

Speleothem $\delta^{13}C$ is regulated by both soil/vegetation processes as well as in-cave processes. The $\delta^{13}C$ of DIC in dripwater is initially set by the $\delta^{13}C$ of soil CO_2, which is more negative when the soil pCO_2 is high under warm and moist conditions which favor high heterotrophic and autotrophic respiration. The $\delta^{13}C$ of DIC in dripwater may be modified slightly during carbonate dissolution, but the low dead carbon percentage in most recent stalagmites, including those from Northern Iberia, suggests that dissolution commonly occurs in open systems and the impact on the $\delta^{13}C$ of DIC is limited (Lechleitner et al., 2021). In the cave or karst cavities, the coupled processes of degassing and PCP can generate a significant positive shift in $\delta^{13}C$ of DIC before the water reaches the stalagmite. The modern $\delta^{13}C_{farmed}$ for the high drip location (-11 to -12‰) is in the range of $\delta^{13}C$ expected for CO_2 in soils with a dominant C3 vegetation in a warm and humid climate (Lechleitner et al., 2021), potentially affected by only limited PCP. The modern $\delta^{13}C_{farmed}$ for the seepage location (MEN-E) and other nearby drips of the same gallery (MEN-F and G) are less negative (-9 to -10‰) and these drips may have experienced some degassing and PCP and/or a greater extent of precipitation from the arriving drip (in situ PCP), and/or a more closed dissolution regime. Seasonal changes in $\delta^{13}C_{farmed}$ at higher and intermediate drip rate sites may reflect seasonal variations in soil pCO_2 or in the significance of PCP. Drip rate monitoring and farmed calcite data suggest that the MEN composite record is not seasonally biased but rather reflects continuous, year-round deposition. Continuous calcite deposition is also supported by the columnar fabric and the absence of visible laminae as well as the lack of dissolution features (i.e., the drip water was always supersaturated with respect to calcite).

Long-term changes in $\delta^{13}C$ values are rather unrelated to the Mg/Ca pattern in the MEN stalagmites. For example, in the $\delta^{13}C$ MEN5 record, the main long-term trends exhibit similar Mg/Ca ratios (low Mg/Ca variability between the different $\delta^{13}C$ larger anomalies; Suppl. Material Fig. S9). Therefore, the temporal trends in $\delta^{13}C$ are most likely driven unaffected by PCP, although the seepage drips may be characterized by some PCP. We suggest that the long-term trends in $\delta^{13}C$ are driven by climatic processes controlling soil pCO_2, i.e. soil temperature and soil moisture. Some studies suggest that the temperature component dominates over soil pCO_2, such during MIS 3 and 4 in Villars cave in SW France (Genty et al., 2006) and during the last deglaciation in El Pindal cave in NW Spain (Moreno et al., 2010). Comparison of the Mendukilo composite $\delta^{13}C$ record with paleotemperature reconstructions from Pyrenean lakes (e.g., Tarrats et al., 2018) and SST records (Català et al., 2019; Martrat et al., 2014) supports a temperature influence at millennial scale (Fig. 5). Therefore, higher (lower) $\delta^{13}C$ values are arguably linked to colder (warmer) and/or dryer (wetter) intervals with reduced (enhanced) soil respiration and vegetation productivity. We note that the inverse correlation between $\delta^{13}C$ and Sr/Ca in the MEN stalagmites (Suppl. Material Fig. S10), while opposite to the trend expected from PCP control, is consistent with the expected relationship of low $\delta^{13}C$ in warm and humid periods of high soil CO_2 which also lead to higher dripwater oversaturation and higher growth rates promoting higher Sr/Ca.

Variation in the dripwater and stalagmite $\delta^{18}O$ record may reflect changes in $\delta^{18}O$ of the surface ocean in the moisture source area, as well as changes in the atmospheric processes which

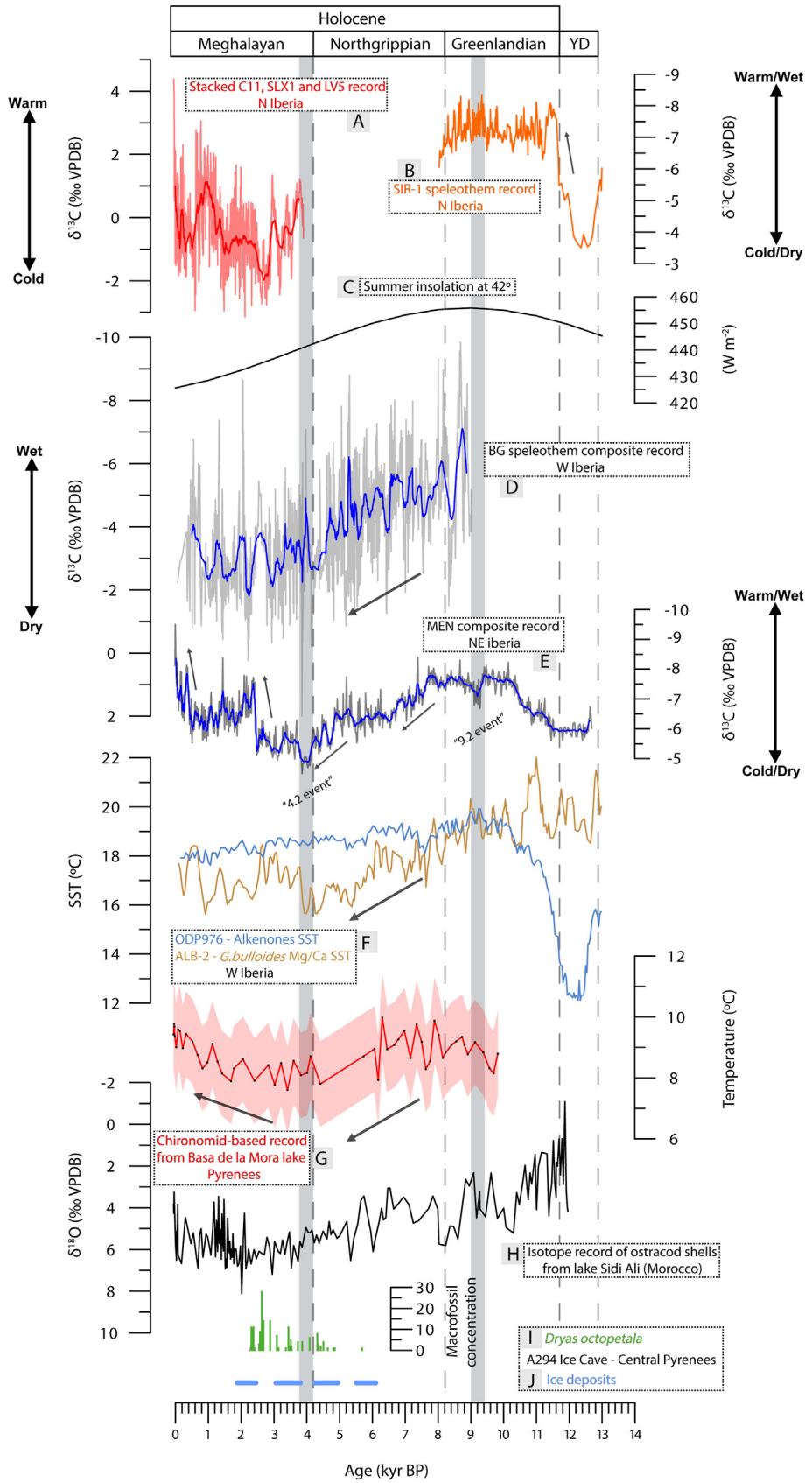

Fig. 5. Pal eoenvironmental records from the Iberian Peninsula and Morocco covering the YD and the Holocene. **A)** Stacked record of normalized $\delta^{13}C$ stalagmite data from Kaite cave; Cueva del Cobre; Cueva Mayor from northern Iberia (Martín-Chivelet et al., 2011). **B)** $\delta^{13}C$ record of the SIR-1 speleothem from El Soplao cave in northern Iberia (Rossi et al., 2018). **C)** Summer insolation at 42°. **D)** $\delta^{13}C$ record of the BG speleothem from westernmost Iberia (Buraca Gloriosa Cave, Portugal) (Thatcher et al., 2020). Note that amplitude of $\delta^{13}C$ axis in this record (high variability) is not the same compared to the rest of Iberian stalagmite records. **E)** MEN $\delta^{13}C$ composite record (this work). **F)** *G. bulloides* Mg/Ca SST (ALB-

together affect the fractionation of $\delta^{18}O$ in the hydrological cycle between the ocean and rainfall over the cave. Over the time period covered by the MEN record, marine records confirm a significant change of $\delta^{18}O_{sw}$ between 13 and 8 kyr (Català et al., 2019; Peck et al., 2006; Skinner and Shackleton, 2006), but smaller variations since 8 kyr (Suppl. Material Fig. S11). This change in seawater composition is likely a significant component of the long-term trend in MEN $\delta^{18}O$ between 11.5 and 8.5 kyr. Short-term changes in seawater composition, not captured by the low-resolution $\delta^{18}O_{sw}$ may also contribute to variation in MEN $\delta^{18}O$, and in the subsequent section we discuss how these may be distinguished from changes due changing isotope fractionation in the hydrological cycle.

For a constant sea-surface composition, event-scale monitoring of the isotopic composition of oxygen in the rainwater ($\delta^{18}O_r$) in different areas of the Iberian Peninsula constrains some of the drivers of hydrological fractionation (Giménez et al., 2021; Moreno et al., 2014, 2021). Air temperature, together with the amount of precipitation, accounts for less than 40% of the variability of $\delta^{18}O_r$ in the transect across the northern Iberian Peninsula all the way to the Balearic Islands. Rather, the synoptic-scale atmospheric circulation plays the dominant role in determining the ranges, values and seasonal distribution of $\delta^{18}O_r$ (Moreno et al., 2021). In fact, the record of $\delta^{18}O_r$ in the northern coastal area of Iberia (Bilbao) during the last four years (Suppl. Material Fig. S2) indicates a minor dependence on temperature ($r = 0.20$) and precipitation ($r = 0.22$; during days with >3 mm of rainfall). This contrasts with the significant correlation between $\delta^{18}O_r$ and air temperature in more inland and high-elevation settings of the Pyrenees (Giménez et al., 2021), where temperature could be interpreted as dominating $\delta^{18}O$ stalagmite records (Bartolomé et al., 2015; Bernal-Wormull et al., 2021). In the northern coastal region, the seasonality of rainfall has been discussed as a potential driver of stalagmite $\delta^{18}O$ (Baldini et al., 2019).

At the Mendukilo cave location, dripwater and farmed calcite provide a limited perspective and suggest that both $\delta^{18}O_{drip}$ and $\delta^{18}O_{farmed}$ are lower during the rainy period 2018–2019 than during the drier year 2020–2021 (Fig. 2). This suggests that synoptic processes during a wet year may lead to lower $\delta^{18}O$ stalagmite. Monitoring and petrographic data thus suggest that the MEN $\delta^{18}O$ record captured an annual signal, which is primarily influenced by rainfall amount as well as by changes in the isotopic composition of the ocean during the first part of the record (13–8 kyr). A prominent feature of the MEN $\delta^{18}O$ composite record is a −0.71‰ anomaly (relative to the Holocene mean of −5.4‰) that repeats at 8.11 kyr BP and at 7.00 kyr BP (Fig. 4). During these time periods, neither $\delta^{13}C$ nor Mg/Ca show a negative shift as might be expected for increased rainfall, nor is did the growth rate increase. Thus, we propose that these two events of anomalously low $\delta^{18}O$ values are likely caused not by increased rainfall amount but rather record rapid and short-lived decreases in $\delta^{18}O_{sw}$ (e.g. Dominguez-Villar et al., 2009; García-Escárzaga et al., 2022; LeGrande and Schmidt, 2008; Matero et al., 2017).

5.2. Climate variability reconstructed for northern Iberia during the YD and the Holocene

5.2.1. Younger Dryas

The YD was a cool and generally dry episode that very likely resulted from a prolonged weakening of the Atlantic Meridional Overturning Circulation (AMOC) (Bakke et al., 2009; McManus et al., 2004). This event is precisely recorded in lake sediments (Gil-Romera et al., 2014; González-Sampériz et al., 2006; Leunda et al., 2017; Morellón et al., 2018) and speleothems (Baldini et al., 2019; Bernal-Wormull et al., 2021; Moreno et al., 2010; Rossi et al., 2018) from northern Iberia confirming its cool and dry character in southwestern Europe. Moreover, a high-resolution Pyrenean speleothem provided evidence of two hydrological contrasting phases within the YD (Bartolomé et al., 2015; Cheng et al., 2020) supporting previous observations from pollen in Iberian marine sediments (e.g., Chabaud et al., 2014; Fletcher et al., 2010; Combourieu-Nebout et al., 2009; Rodrigues et al., 2010). In Mendukilo cave, the lowest speleothem growth rates of the entire record were recorded during the YD (29–37 μm/yr), while the composite MEN $\delta^{13}C$ record (Figs. 4 and 5) shows higher values (−6.0‰) in relation to the average $\delta^{13}C$ value of the Greenlandian (−7.2‰). These data provide evidence of dry and cold conditions during the YD in this region which would have resulted in slow speleothem growth (low Sr/Ca ratio) and elevated $\delta^{13}C$ values. Similarly, mean values of the MEN $\delta^{18}O$ (Fig. 4) composite record are slightly lower (−5.0‰) than at the beginning of the Holocene (−4.7‰). As also observed by Baldini et al. (2019) in La Garma cave, YD $\delta^{18}O$ values in Mendukilo record are not particularly different from other Holocene intervals where $\delta^{18}O$ values are even lower (e.g., $\delta^{18}O$ values of −5.8‰ at 7.87 ka BP, compared to a value of −5.4‰ at 12.29 ka BP). Baldini et al. (2019), using a Monte Carlo model applied to the GAR-01 $\delta^{18}O$ record, report that seasonal rainfall and temperature distribution account for 95% of the $\delta^{18}O$ variability and that the YD was characterized by dry and cool winters and wet summers. Thus, the $\delta^{18}O$ values recorded in Mendukilo during the YD are actually higher than expected if they were recording cold temperatures given the decrease in winter precipitation. Besides this combination of climate variables, those higher $\delta^{18}O$ values may be related to the higher $\delta^{18}O_{sw}$ values that characterize North Atlantic records in the YD (Suppl. Material Fig. S11) thus enforcing the idea that the MEN record captured important changes in the isotopic composition of the North Atlantic Ocean.

Regarding the intra-YD variability, the MEN $\delta^{13}C$ composite suggests a quite stable YD in terms of soil and vegetation activity. On the contrary, the MEN $\delta^{18}O$ composite shows three different phases, in good correspondence with a simplified version of the three stages recorded by marine sediments (Naughton et al., 2019): (i) a cool/dry climate at the YD onset, (ii) a slightly warmer (and wetter) phase at about 12.3 kyr BP, and (iii) a cool and dry (but quite unstable phase) just before the onset of the Holocene. The age model (Fig. 3B) precludes establishing the precise timing of these stages. The fact that this intra-YD variability is observed in the $\delta^{18}O$ but not in the $\delta^{13}C$ data may provide a hint to the season when most of the rain fell. If there was enough rainfall in the warm season (spring-summer, as proposed by Baldini et al., 2019) to support vegetation growth and soil activity, then the $\delta^{13}C$ may have remained stable during the YD while the $\delta^{18}O$ values oscillated. Thus, a change in rainfall seasonality during the YD may explain the different patterns of carbon and oxygen isotopes from Mendukilo cave, as previously suggested for La Garma cave (Baldini et al., 2019). Similar ideas about the proxy expression of the YD seasonality may be reflected by SST proxies in Fig. 5F. Thus, SST obtained from Mg/Ca (Català et al., 2019) presents a much less pronounced temperature change during the YD than SST obtained from alkenones (Martrat et al., 2004).

2; Català et al., 2019) compared with the alkenone SST (Martrat et al., 2014) from West Mediterranea. **G)** Temperature record of the Basa de la Mora lake in the Central Pyrenees based on chironomid data (Tarrats et al., 2018) **H)** $\delta^{18}O$ values of ostracod shells from lake Sidi Ali (Morocco; Zielhofer et al., 2019). **I)** *Dryas octopetala* macrofossil abundance (Leunda et al., 2019) and **J)** phases of ice accumulation (Sancho et al., 2018) in the Armeña-A294 Ice Cave (Central Pyrenees). The Holocene is divided following Walker et al. (2019). The "4.2 and the 9.2 events" are indicated by higher values in the MEN $\delta^{13}C$ composite record (this work).

5.2.2. Onset of the Holocene and the Greenlandian period

The onset of the Holocene has not been well captured by Iberian speleothems as most of them started to grow after 10–9.5 kyrs BP (Railsback et al., 2011; Stoll et al., 2013; Walczak et al., 2015), once optimum climatic conditions in terms of temperature and humidity were attained. Even so, there are few speleothem records in northern Spain that cover the climate transition between the YD and the Holocene (Baldini et al., 2015, 2019; Bernal-Wormull et al., 2021; Moreno et al., 2017; Rossi et al., 2018). In the case of Mendukilo cave, there is only one stalagmite, MEN-2, which started to grow just before the YD and continuously covers the Holocene until 6 kyr BP. Its $\delta^{13}C$ and $\delta^{18}O$ profiles show a slower transition until optimum conditions are reached (Fig. 4, Fig. S4 and Fig. S5). Thus, the MEN $\delta^{13}C$ isotope composite records a different signal at the Holocene onset compared to speleothems from NW Iberia, such as the SIR-1 speleothem from El Soplao cave (Rossi et al., 2018) (Fig. 5B), a record that reflects an (hydro)climate signal as well as the MEN $\delta^{13}C$ composite between intervals of cold/dry or warm/wet conditions. In the case of SIR-1, the $\delta^{13}C$ values decrease quickly at the end of the YD and remain stable throughout the Greenlandian (Fig. 5B). On the other hand, the $\delta^{13}C$ profile in Mendukilo shows a gradual positive trend since the end of the YD lasting until 10 kyr BP when $\delta^{13}C$ values stabilize (Fig. 5E). This difference in the $\delta^{13}C$ signal of both records may be due the fact multiple studies show that Holocene humidity changes are locally variable and of contrasting sign between NW, eastern and southern Iberia (Morellón et al., 2018) allowing the Mendukilo record to be affected not only by a purely Atlantic signal, but rather a combination of a Mediterranean (where several records in the region show a delay in reaching Holocene optimum conditions) and Atlantic signal. Another possibility is that the hydrological imprint is predominant in the case of MEN stalagmites to the detriment of temperature as in the case of SIR-1. Coherently, the $\delta^{18}O$ MEN record shows the least negative values of the whole record at the onset of the Holocene, when temperatures were high but water availability was still low and $\delta^{18}O_{sw}$ still shows highly positive values (Suppl. Material Fig. S11). The $\delta^{18}O$ values then gradually decrease until 8 kyr, which coincides not only with the change towards optimal conditions during the beginning of the Holocene, but also with a significant evolution of $\delta^{18}O_{sw}$ in marine records between 11 and 8 kyr BP (Suppl. Material Fig. 11) as a result of meltwater pulses in the North Atlantic (Peck et al., 2006; Skinner and Shackleton, 2006) (Fig. 4). Another point to consider is that the relevant increase in temperature during the early Holocene must necessarily modify the $^{18}O/^{16}O$ fractionation in the cave, which could lead to a progressive but very significant decrease in the $\delta^{18}O$ of the speleothem. Rainfall monitoring surveys in the Central Pyrenees indicate that $\delta^{18}O$ values in precipitation ($\delta^{18}O_p$) show a dependence of temperature equivalent to a temperature dependence on $\delta^{18}O_p$ of 0.47–0.52‰/°C (Bartolomé et al., 2015). This dependence is only partially offset by the empirical change of the value of isotope fractionation during calcite precipitation (Tremaine et al., 2011). Therefore, attributing the progressive decline in $\delta^{18}O$ values purely to changes in fractionation does not seem feasible. Therefore, both isotopic records, together with Sr/Ca ratios and growth rates (which increase from 40 to 63 μm/yr; Fig. 3 and Fig. S10) support the model of a progressive change towards more humid conditions from the onset of the Holocene to 10.5–10.0 kyr BP, coinciding with the start of the Holocene Thermal Maximum at higher latitudes (Marcott et al., 2013). From 10 to 8 kyr BP, optimum conditions in terms of soil activity and vegetation development were attained around Mendukilo cave (Fig. 4). Regarding SST, that interval also correspond with the highest temperatures of the Holocene (Fig. 5F).

Morellón et al. (2018) compiled lake and speleothem records from Iberia covering the Holocene onset and observed two main patterns of spatial and temporal hydrological variability: i) Atlantic-influenced sites located in the Northwest (e.g., Enol or Sanabria lakes, Moreno et al., 2011; Jambrina-Enríquez et al., 2014) and speleothems from the Cantabrian coast (Stoll et al., 2013) are characterized by a gradual increase in humidity from the end of the YD to the mid Holocene, similarly to most North Atlantic records; and ii) continental and Mediterranean-influenced sites (e.g., Villarquemado or Estanya lake, Aranbarri et al., 2014; Morellón et al., 2009 and El Refugio cave; Walczak et al., 2015) show evidence of prolonged arid conditions of variable duration after the YD, followed by an abrupt increase in moisture at 10-9 kyr BP. Mendukilo cave, showing a gradual increase in moisture availability since the end of the YD, falls into the first category. This delay in reaching optimum temperature and humidity conditions during the Holocene agrees with the insolation change at this latitude, which reaches its maximum approximately at 10 kyr BP (Fig. 5C). Optimum humidity conditions in the MEN composite record are maintained between 10 and 7.8 kyr BP, contrary to what is seen in speleothems from the Mediterranean part which suggest an arid climate at that time (Budsky et al., 2019).

5.2.3. From the Northgrippian to the end of the Neoglacial cooling

The Northgrippian (8.2–4.2 kyr BP) was characterized by a gradual increase in the MEN $\delta^{13}C$, with centennial-scale oscillations, pointing to the end of optimum thermal and humidity conditions in the region (Figs. 4 and 5). This trend was accompanied by a decrease in growth rate of the MEN stalagmites (Fig. 3 and Suppl. Material Fig. S8 and Fig. S10) while speleothem growth in southern Iberia stopped (Walczak et al., 2015). Generally dry conditions across much of Iberia between ca. 8 to 5 kyr BP are suggested by positive $\delta^{13}C$ excursions in the northwest Iberian Cova de Arcoia (Railsback et al., 2011), the GAR-01 stalagmite (Baldini et al., 2019), stalagmites from caves in the Iberian range growing during 8.5–4.8 ka (Moreno et al., 2017) and a sharp decrease of precipitation derived from growth rates of 11 stalagmites on the Cantabrian coast (Stoll et al., 2013). Similarly, the long-term trend in carbon and oxygen isotopic variability of the composite record of six stalagmites from Buraca Gloriosa (BG) in western Portugal (Thatcher et al., 2020) suggests drier conditions from the middle to late Holocene as evidenced by increasing $\delta^{13}C$ and $\delta^{18}O$ values (Fig. 5D). Lake records from Spain (González-Sampériz et al., 2017; Jambrina-Enríquez et al., 2014; Moreno et al., 2011) and a pollen-based climate reconstruction from Mauri et al. (2015), as well as a lacustrine $\delta^{18}O$ record from Morocco (Zielhofer et al., 2019, Fig. 5H) support increasingly dry conditions in Iberia and North Africa during the Northgrippian. This trend mimics the long-term trend of decreasing values in summer insolation (Fig. 5C). Dry conditions, however, were not reached at the same time at all sites. These proxy records suggest that during the mid-Holocene aridity prevailed in both southern and north-western Iberia, while moisture availability in the north was likely higher (probably controlled by the winter westerlies) than in southern Iberia, reflected by the continuous growth of northern (Baldini et al., 2019; this work) relative to southern stalagmites between ca. 8 to 5 kyr BP (Walczak et al., 2015).

The Northern Hemisphere experienced a wide-spread cooling starting at about 6.0–5.5 kyr BP known as the Neoglacial period (Davis et al., 2009; Kumar, 2011). This trend is captured by the MEN $\delta^{13}C$ composite record (Fig. 5E) with a trend towards less negative values starting about 5.2 kyr BP. This cooling is known throughout Europe (e.g., Ilyashuk et al., 2011; Larocque-Tobler et al., 2010) and, regarding Iberian records, is documented by *G. bulloides* Mg/Ca SST from the Alboran Sea (Català et al., 2019, Fig. 5F) and the continental chironomid-based temperature reconstruction from la Basa de la Mora in central Pyrenees (Tarrats et al., 2018, Fig. 5G). Glaciers

began to expand around 6 kyr BP in both the southern (García-Ruiz et al., 2020) and the northern (Gellatly et al., 1992) part of the Pyrenees and Arctic–Alpine species such as *Dryas octopetala* spread (Leunda et al., 2019, Fig. 5I) simultaneous with the accumulation of ice in caves at high elevation in the central Pyrenees (Sancho et al., 2018, Fig. 5J).

The onset of the Meghalayan at 4.2 kyr BP coincides with higher isotopic values in the MEN composite $\delta^{13}C$ record (Fig. 5E) in comparison with what was seen during the Northgrippian period. This trend ends around 2.5 kyr BP, when a gradual amelioration led to the onset of a relatively warmer and/or humid interval, in agreement with the Basa de la Mora lake record (Fig. 5G) and the Mg/Ca SST marine records (Fig. 5F). Besides, the MEN $\delta^{18}O$ composite values stabilized around −5.2‰ 5 kyr BP ago (punctuated by centennial-scale oscillations), likely reflecting the combination of cold and dry conditions. Thus, cold and probably dry conditions prevailed in northern Iberia between the onset of Neoglacial at about 5–6 kyr BP and 2.5 kyr BP.

After 2.5 kyr BP, a gradual amelioration trend led to relatively warmer and/or humid conditions which lasted until ~1700 yr BP as recorded by the $\delta^{13}C$ MEN composite and the increase in growth rate (Fig. 5 and Fig. S10, Suppl. Mat.). The last 2.5–3 kyr, however, are not well-resolved in the MEN record (Fig. S4, Suppl. Mat.) and climate inferences are less robust than for the earlier part of the record.

5.3. Abrupt climate changes during the Holocene

Although the $\delta^{18}O$ variability of the MEN record is small throughout the Holocene, as the case of most records in the region (Baldini et al., 2019; Dominguez-Villar et al., 2009; Smith et al., 2016), we identified four events of lower $\delta^{18}O$ values (at 8.2, 7.0–6.6, 5.5–4.8, and 2.8 kyr BP) that can be correlated within dating uncertainty with other cave records and compared with some of the Bond events, periods with increase of North Atlantic ice-rafted debris record in marine sediment cores (Bond et al., 2001) (stacked MC52, VM29–191, MC21 and GGC22 marine cores) (Fig. 6). These negative excursions along the Holocene MEN $\delta^{18}O$ composite curve (representing centennial scale cold events) can be compared with maxima in the ice-rafted debris record (cold meltwater input at the north Atlantic) despite to different resolutions and probable uncertainties in both age models. Other abrupt hydroclimatic changes during the Holocene that have been identified in Iberian records occurred at 9.2 and 4.2 kyr BP (Baldini et al., 2019; Jiménez-Moreno et al., 2015; Mesa-Fernández et al., 2018; Walczak et al., 2015). These two events are not prominent in the $\delta^{18}O$ MEN record, but both are clearly expressed in the $\delta^{13}C$ record (Fig. 5). Those six Holocene events are discussed separately since their origin and signal is not the same.

5.3.1. The 9.2 kyr BP event

Between 8.9 and 9.3 kyr BP the MEN $\delta^{13}C$ composite values increase (amplitude of 1‰) coinciding with the '9.2 kyr event' (Fig. 5), documented in many proxy records across the Northern Hemisphere (e.g., Fleitmann et al., 2008; Genty et al., 2006; Masson-Delmotte et al., 2005; Rasmussen et al., 2007). This event may reflect the effects of a meltwater pulse (Fleitmann et al., 2008). Indeed, a major $\delta^{18}O$ peak in the lake sediment record of Sidi Ali, Morocco (Zielhofer et al., 2019), coincides with maxima in ice-rafted debris in the North Atlantic at 9.3 kyr BP (Bond, 1997). This prominent peak (Fig. 5H) corresponds to Bond event 6 (Bond, 1997; Bond et al., 2001). Mesa-Fernández et al. (2018) identified a short and relatively arid in the Laguna Hondera record (southern Iberian Peninsula) between ~ 9.6 and 9.0 kyr BP. As indicated above, this event is not reflected in the MEN composite $\delta^{18}O$ signal (not even in the $\delta^{18}O$ values of the MEN-2 stalagmite separately; Fig. S5) but in its $\delta^{13}C$ record. A possible explanation is that the drier conditions, documented for this period for the Iberian Peninsula by terrestrial (Baldini et al., 2019; Carrión, 2002; Iriarte-Chiapusso, 2016; Vegas et al., 2010) and marine records (Combourieu-Nebout et al., 2009), played a role in counteracting this MEN $\delta^{18}O$ composite signal, in a similar way to what we have seen in the $\delta^{18}O$ values of the MEN record during the cold and dry YD (Fig. 6A). Baldini et al. (2019) suggested arid summers between 9.3 and 8.9 kyr BP, roughly corresponding to our "9.2 kyr event", based on modelled seasonality data (Fig. 6D). This summer aridity suggests that a Mediterranean-type climate may have existed in northern Iberia at this time, which is also consistent with the northward shift of the westerly (Walczak et al., 2015). This movement results in an increase in moisture observed in Scandinavia (Bakke et al., 2009) and a reduction of moisture in southern France (Genty et al., 2006; Wirth et al., 2013) and northern Iberia (Aranbarri et al., 2014; Railsback et al., 2011).

5.3.2. The 8.2 kyr BP event

One of the largest depletion in $\delta^{18}O$ values recorded by the MEN composite and stalagmites MEN-2 and MEN-5 occurred between 8.1 and 8.2 kyr BP (amplitude of 0.6‰) (Fig. 6 and Fig. S5), coinciding with the so-called '8.2 kyr event' (Alley et al., 1997). This larger depletion in the composite record presents a similar chronology and intensity in the $\delta^{18}O$ individual records of the MEN-2 and MEN-5 stalagmites (Fig. S5). Catastrophic meltwater during the '8.2 event' from Agassiz glacial lake dropped the North Atlantic isotope composition of the surface water by 0.4‰ (Carlson et al., 2008; Kleiven et al., 2008) that according to cooling of the North Atlantic region. This regional cooling is well described for this event (R. Alley and Agustsdottir, 2005; Ayache et al., 2018) and resulted in a fresh $\delta^{18}O_{sw}$ signal that was transferred into the precipitation of the region (LeGrande and Schmidt, 2008). Many Iberian speleothem captured a negative $\delta^{18}O$ anomaly during this time (Baldini et al., 2019; Benson et al., 2021; Dominguez-Villar et al., 2009; Kilhavn et al., 2022; Thatcher et al., 2020), possible growth hiatuses (e.g., Asiul Cave - ASR; El Soplao Cave - SIR-1) and even erosion events (e.g., Cova da Arcoia - ESP03), thus revealing a coherent regional response to this event. Thatcher et al. (2020) summarized hydroclimate data for Iberia between 8.8 and 8.0 kyr BP, signaling the difference between south and north (humid or variable) in relation to the central and westermost (arid) zone of Iberia in terms of humidity. The 8.2 kyr event is pronounced in the MEN $\delta^{18}O$ composite record, in contrast to the 9.2 kyr BP event. The conditions in northern Iberia were therefore colder and with a contribution of freshwater from the North Atlantic in the negative signal of $\delta^{18}O_{sw}$. This allows the cold anomaly of the 8.2 kyr event to be clearly expressed in the MEN $\delta^{18}O$ record.

5.3.3. The 7.0–6.6 kyr and 5.5–4.8 kyr BP events

The next event of anomalously low $\delta^{18}O$ values occurred between 7.0 and 6.6 kyr BP (Fig. 6 and Fig. S5), with a very similar intensity as the one at 8.1 kyr BP (reaching values of −5.98 in the MEN-2 stalagmite, −6.33 in the $\delta^{18}O$ values of the MEN-5 stalagmite and −6.23‰ in the MEN $\delta^{18}O$ composite record). This event in MEN may be associated to meltwater pulse during the final demise of the Laurentide ice sheet, which disappeared at 7 kyr BP (Carlson et al., 2008) and correlates quite well with the BG speleothem record (Thatcher et al., 2020, Fig. 6C) and the LV5 record (Dominguez-Villar et al., 2009, Fig. 6C). Between 5.5 and 4.8 kyr BP the stalagmites MEN-3 and MEN-5 (and the MEN $\delta^{18}O$ composite) shows small drops in $\delta^{18}O$, an event which is more evident in W Iberia (BG record; Thatcher et al., 2020) and NW African lakes (Sidi Ali $\delta^{18}O$ values; Zielhofer et al., 2019) reflecting the last part of Bond event 4

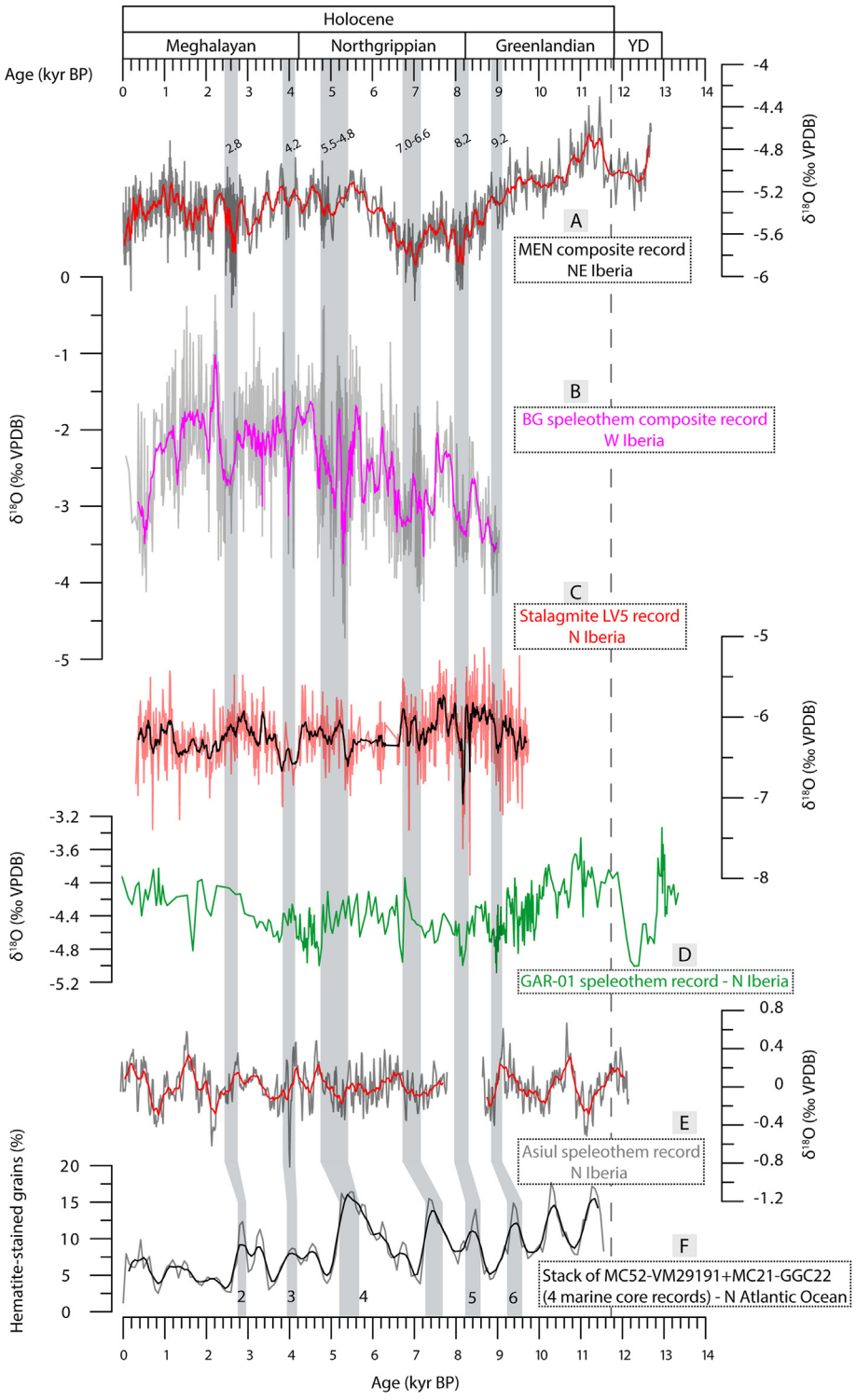

Fig. 6. $\delta^{18}O$ records from the Iberian Peninsula showing evidence of abrupt climate change in the Holocene. **A)** MEN $\delta^{18}O$ speleothem composite (this work). **B)** $\delta^{18}O$ record of the BG speleothem from westernmost Iberia (Buraca Gloriosa Cave, Portugal) (Thatcher et al., 2020). **C)** $\delta^{18}O$ record of LV5 stalagmite from northern Iberia (Kaite Cave) (Domínguez-Villar et al., 2017). **D)** GAR-01 speleothem record from northern Iberia (La Garma Cave) (Baldini et al., 2019). The vertical grey bars mark abrupt events within the Holocene. **E)** Combined and normalized Cueva de Asiul speleothem $\delta^{18}O$ data from northern Iberia (Smith et al., 2016). **F)** Ice-rafted debris (IRD) record based on hematite-stained grains of stacked MC52, VM29–191, MC21 and GGC22 cores from the subpolar North Atlantic (Bond et al., 2001). Note that the amplitude of $\delta^{18}O$ axis is not the same for the case of MEN composite record (low variability) in comparison with the rest of the $\delta^{18}O$ records.

(Fig. 6F). Thatcher et al. (2020) argued that on a centennial scale, increased effective precipitation in westernmost Iberia, indicated by lower stalagmite $\delta^{13}C$ and $\delta^{18}O$ values, is evident at 7.5–7.1, 6.9–6.5, 6.4–6.0, 5.5–5.2 kyr BP at BG (Figs. 5D and 6B). However, those events were identified as arid phases (7.5–7.0 and 5.5–5.0 kyr BP) in the FUENT-1 lacustrine sequence from central Iberia

(Vegas et al., 2010) and in the Laguna Hondera record from southern Iberia (Mesa-Fernández et al., 2018). The fact that these short intervals are observed in several records within this region indicating humid conditions in the north and drier conditions in the south highlights the different hydroclimate response across west/northern Iberia compared to central/southern Iberia during the Northgrippian (Thatcher et al., 2020). A similar latitudinal pattern was described for the Central Mediterranean by Magny et al. (2013) signaling changes in the seasonality of precipitation as the main cause of differences between northern and southern Italy.

5.3.4. The 4.2 kyr BP event

The 4.2 kyr event might correspond to Bond event 3 (Fig. 6F), and there is an ongoing debate in the scientific community about the global extent of this cold, dry and locally also dusty multi-centennial event. Evidence of environmental and climatic deterioration around or coincident with the 4.2 kyr BP Event in the Mediterranean Basin is apparent but chronologically compromised considering a different selection of continental and marine records (Bini et al., 2019). According to Smith et al. (2016), based on the speleothem record from Asiul cave in northern Iberia, this dry interval was synchronous with North Atlantic cooling. In southern Spain, another speleothem record revealed a microhiatus at 4.16 kyr that might correspond to the 4.2 kyr event (Walczak et al., 2015). These findings are supported by a pollen record from the Doñana National Park in southwestern Spain that indicates a multi-centennial aridification trend centered at 4.0 kyr cal BP (Jiménez-Moreno et al., 2015). Furthermore, a speleothem record from Gueldaman Cave in northern Algeria revealed a multi-centennial dry phase that started around 4.4 kyr and was synchronous with the human abandonment of the cave (Ruan et al., 2016). Further, there is evidence of increased storm activity in the Mediterranean Basin between 4.4 and 4.0 kyr BP (Kaniewski et al., 2016). Therefore, this dry event was widespread in the Mediterranean region, even reaching the Atlantic part of Iberia.

The 4.2 kyr event is poorly expressed in the MEN $\delta^{18}O$ data (Fig. 6 and Fig. S5). It is likely that this event was more arid than previous events, such as the 8.2 or the 7.1 kyr BP event whereby the strongly negative $\delta^{18}O$ values point to cold temperatures. These arid conditions can act counteracting the MEN composite $\delta^{18}O$ variability. Therefore, the MEN composite recorded cold and very dry conditions during the 4.2 kyr event.

5.3.5. The 2.8 kyr BP event

In the middle of the Meghalayan period there was a 450-year interval (2850–2400 yr BP) of $\delta^{18}O$ values lower than the Holocene mean of the MEN composite record and stalagmites MEN-3, MEN-4 and MEN-5. This $\delta^{18}O$ anomaly is quite noticeable in the MEN-3 record and more subordinate in the case of MEN-4 and MEN-5 (in which it is centered at 2.4 kyr BP) and suggests a period of cooler conditions that can be correlated with the first cold phase of the Subatlantic period, also called the "Iron Age Cold Epoch" (Van Geel et al., 1996). This period has been recognized by Desprat et al. (2003) in sediments from the Ría de Vigo on the northwestern coast of Spain, in a speleothem $\delta^{13}C$ record from northern Spain (Martín-Chivelet et al., 2011), from different areas and proxies in central and western Europe (e.g., Blaauw et al., 2004; Plunkett and Swindles, 2008; Speranza et al., 2003; Van Geel et al., 1996) and Greenland (O'Brien et al., 1995), and was also identified as the ice-rafted debris event 2 (~2700 yr BP) in Atlantic sediment cores (Bond, 1997; Bond et al., 2001) (Fig. 6F). Several hypothesis have considered to explain this cold event, but likely changes in solar activity were one of the dominant forcings, as proposed by Zielhofer et al. (2017). Indeed, the onset of this episode coincided with a minimum in solar activity at ~2800 yr BP (e.g., Swindles et al., 2007; Usoskin et al., 2007).

6. Conclusions

The Mendukilo cave isotopic record, composed of four stalagmites dated at high precision, provides replicated and continuous speleothem information from the northern Iberian Peninsula for the YD and the entire Holocene able to capture centennial-multidecadal climate variability. Changes in the MEN $\delta^{13}C$ composite record are principally driven by climatic processes controlling soil pCO_2 and not by in-cave processes. This is supported by the variability of Sr/Ca (influenced by the growth rate) which is negatively correlated with the MEN $\delta^{13}C$ values. Carbon isotope values of the MEN composite display a high variability that correlates well with other records in the region with respect to changes in humidity and/or temperature related to insolation variability and North Atlantic climate. Thus, high MEN $\delta^{13}C$ values in the composite record during the YD indicate drier and colder conditions which resulted in low speleothem growth rates (low Sr/Ca ratios). The $\delta^{13}C$ data indicate a progressive change towards more humid conditions between the onset of the Holocene and 10–10.5 kyr BP, which represents a delayed signal with respect to climate warming at the Holocene onset (i.e. at 11.7 kyr BP). The onset of the Northgrippian marks the end of the climate optimum in the region and a tendency towards a drier climate which culminated in the Neoglacial, a cold and dry period between 6.0 and 2.5 kyr BP.

The oxygen isotope data of the MEN record show low variability, such as other speleothem records from the region, and especially negative values during some short events (eg. 8.2 kyr BP) which are synchronous within age uncertainties with abrupt changes associated with AMOC perturbations and/or meltwater discharges into the North Atlantic and concomitant changes in the isotopic composition of the North Atlantic surface waters. This relationship between MEN $\delta^{18}O$ and $\delta^{18}O_{sw}$ is also evident at millennial scale at the beginning of the Holocene, where the progressive change towards less negative values correlates well with marine isotopic records in the North Atlantic. Regarding the centennial scale, the MEN oxygen isotope composite records cold events at 8.2, 7.0–6.6, 5.5–4.8 and 2.8 kyr BP associated with major disturbances in the North Atlantic deep-water circulation and sometimes as result of meltwater input (at least for the first two events). Other two events, the 9.2 kyr and the 4.2 kyr events, are not captured by the MEN $\delta^{18}O$ profile but clearly expressed in the $\delta^{13}C$ profile. We interpret these events as dominated by dry and cold conditions (instead of wet and cold) where temperature and humidity changes have competing effects on the $\delta^{18}O$ signal.

Author contributions

J. L. Bernal-Wormull; A. Moreno; M. Bartolomé; C. Pérez-Mejías; M. Arriolabengoa: Contributed to design this research project. **C. Spötl:** Provided the isotopic data. **R.L. Edwards; H. Cheng:** Provided the chronological data. **E. Iriarte; C. Osácar:** Provided the thin sections and contributed in the petrographic characterization. **A. Moreno; C. Pérez-Mejías; M. Bartolomé; M. Arriolabengoa:** Helped during field work. All authors contributed to the writing of the manuscript.

Declaration of competing interest

The authors declare that they have no known competing financial interests or personal relationships that could have appeared to influence the work reported in this paper.

Data availability

Data will be made available on request.

Acknowledgments

We acknowledge the Spanish projects PID 2019–106050RB-I00 (PYCACHU) and CGL 2016-77479-R (SPYRIT), the National Natural Science Foundation of China (NSFC) grants 41888101 and 42050410317, and the Postdoctoral Science Foundation of China (2020M683452) for funding. J.L. Bernal-Wormull was supported by an FPI grant (ref. BES-2017–081125). We are grateful to the guides and workers of the Mendukilo cave, M. Larburu and A. Govillar, for helping with the monitoring work in the cave and preserving the sampling points. We are also grateful to P. Töchterle and M. Wimmer for support during lab work at Innsbruck University, and to all people who helped during field work. We would like to acknowledge the use of Servicio de Apoyo a la Investigación, Zaragoza and the staff of the IsoTOPIK laboratory at University of Burgos. I. Cacho thanks the Catalan Institution for Research and Advanced Studies (ICREA) academia program from the Generalitat de Catalunya.

Appendix A. Supplementary data

Supplementary data to this article can be found online at https://doi.org/10.1016/j.quascirev.2023.108006.

References

Allen, J.R.M., Huntley, B., Watts, W.A., 1996. The vegetation and climate of northwest Iberia over the last 14,000 years. J. Quat. Sci. 11 (2), 125–147. https://doi.org/10.1002/(SICI)1099-1417(199603/04)11:2<125::AID-JQS232>3.0.CO;2-U.

Alley, R., Agustsdottir, A., 2005. The 8k event: cause and consequences of a major Holocene abrupt climate change. Quat. Sci. Rev. 24 (10–11), 1123–1149. https://doi.org/10.1016/j.quascirev.2004.12.004.

Alley, R.B., Mayewski, P.A., Sowers, T., Stuiver, M., Taylor, K.C., Clark, P.U., 1997. Holocene climatic instability: a prominent, widespread event 8200 yr ago. Geology 25 (6), 483. https://doi.org/10.1130/0091-7613(1997)025<0483:HCIAPW>2.3.CO;2.

Aranbarri, J., González-Sampériz, P., Valero-Garcés, B., Moreno, A., Gil-Romera, G., Sevilla-Callejo, M., García-Prieto, E., Di Rita, F., Mata, M.P., Morellón, M., Magri, D., Rodríguez-Lázaro, J., Carrión, J.S., 2014. Rapid climatic changes and resilient vegetation during the Lateglacial and Holocene in a continental region of south-western Europe. Global Planet. Change 114, 50–65. https://doi.org/10.1016/j.gloplacha.2014.01.003.

Ayache, M., Swingedouw, D., Mary, Y., Eynaud, F., Colin, C., 2018. Multi-centennial variability of the AMOC over the Holocene: a new reconstruction based on multiple proxy-derived SST records. Global Planet. Change 170, 172–189. https://doi.org/10.1016/j.gloplacha.2018.08.016.

Bakke, J., Lie, Ø., Heegaard, E., Dokken, T., Haug, G.H., Birks, H.H., Dulski, P., Nilsen, T., 2009. Rapid oceanic and atmospheric changes during the Younger Dryas cold period. Nat. Geosci. 2 (3), 202–205. https://doi.org/10.1038/ngeo439.

Baldini, L.M., Baldini, J.U.L., McDermott, F., Arias, P., Cueto, M., Fairchild, I.J., Hoffmann, D.L., Mattey, D.P., Müller, W., Nita, D.C., Ontañón, R., García-Moncó, C., Richards, D.A., 2019. North Iberian temperature and rainfall seasonality over the younger Dryas and Holocene. Quat. Sci. Rev. 226, 105998. https://doi.org/10.1016/j.quascirev.2019.105998.

Baldini, L.M., McDermott, F., Baldini, J.U.L., Arias, P., Cueto, M., Fairchild, I.J., Hoffmann, D.L., Mattey, D.P., Müller, W., Nita, D.C., Ontañón, R., García-Moncó, C., Richards, D.A., 2015. Regional temperature, atmospheric circulation, and sea-ice variability within the Younger Dryas Event constrained using a speleothem from northern Iberia. Earth Planet Sci. Lett. 419, 101–110. https://doi.org/10.1016/j.epsl.2015.03.015.

Bartolomé, M., Sancho, C., Moreno, A., Oliva-Urcia, B., Belmonte, á., Bastida, J., Cheng, H., Edwards, R.L., 2015. Upper pleistocene interstratal piping-cave speleogenesis: the Seso cave system (central Pyrenees, northern Spain). Geomorphology 228, 335–344. https://doi.org/10.1016/j.geomorph.2014.09.007.

Benson, A., Hoffmann, D. L., Daura, J., Sanz, M., Rodrigues, F., Souto, P., & Zilhão, J. (s. f.). A speleothem record from Portugal reveals phases of increased winter precipitation in western Iberia during the Holocene. The Holocene, 12.

Bernal-Wormull, J.L., Moreno, A., Pérez-Mejías, C., Bartolomé, M., Aranburu, A., Arriolabengoa, M., Iriarte, E., Cacho, I., Spötl, C., Edwards, R.L., Cheng, H., 2021. Immediate temperature response in northern Iberia to last deglacial changes in the North Atlantic. Geology 49 (8), 999–1003. https://doi.org/10.1130/G48660.1.

Bini, M., Zanchetta, G., Perşoiu, A., Cartier, R., Català, A., Cacho, I., Dean, J.R., Di Rita, F., Drysdale, R.N., Finnè, M., Isola, I., Jalali, B., Lirer, F., Magri, D., Masi, A., Marks, L., Mercuri, A.M., Peyron, O., Sadori, L., et al., 2019. The 4.2 ka BP Event in the Mediterranean region: an overview. Clim. Past 15 (2), 555–577. https://doi.org/10.5194/cp-15-555-2019.

Blaauw, M., van Geel, B., van der Plicht, J., 2004. Solar forcing of climatic change during the mid-Holocene: indications from raised bogs in The Netherlands. Holocene 14 (1), 35–44. https://doi.org/10.1191/0959683604hl687rp.

Bond, G., 1997. A pervasive millennial-scale cycle in North Atlantic Holocene and glacial climates. Science 278 (5341), 1257–1266. https://doi.org/10.1126/science.278.5341.1257.

Bond, G., Kromer, B., Beer, J., Muscheler, R., Evans, M.N., Showers, W., Hoffmann, S., Lotti-Bond, R., Hajdas, I., Bonani, G., 2001. Persistent solar influence on North Atlantic climate during the Holocene. Science 294 (5549), 2130–2136. https://doi.org/10.1126/science.1065680.

Budsky, A., Scholz, D., Wassenburg, J.A., Mertz-Kraus, R., Spötl, C., Riechelmann, D.F., Gibert, L., Jochum, K.P., Andreae, M.O., 2019. Speleothem δ^{13}C record suggests enhanced spring/summer drought in south-eastern Spain between 9.7 and 7.8 ka – a circum-Western Mediterranean anomaly? Holocene 29 (7), 1113–1133. https://doi.org/10.1177/0959683619838021.

Carlson, A.E., LeGrande, A.N., Oppo, D.W., Came, R.E., Schmidt, G.A., Anslow, F.S., Licciardi, J.M., Obbink, E.A., 2008. Rapid early Holocene deglaciation of the Laurentide ice sheet. Nat. Geosci. 1 (9), 620–624. https://doi.org/10.1038/ngeo285.

Carrión, J.S., 2002. Patterns and processes of Late Quaternary environmental change in a montane region of southwestern Europe. Quat. Sci. Rev. 21 (18–19), 2047–2066. https://doi.org/10.1016/S0277-3791(02)00010-0.

Carrión, J.S., Fernández, S., González-Sampériz, P., Gil-Romera, G., Badal, E., Carrión-Marco, Y., López-Merino, L., López-Sáez, J.A., Fierro, E., Burjachs, F., 2010. Expected trends and surprises in the lateglacial and Holocene vegetation history of the Iberian Peninsula and Balearic Islands. Rev. Palaeobot. Palynol. 162 (3), 458–475. https://doi.org/10.1016/j.revpalbo.2009.12.007.

Català, A., Cacho, I., Frigola, J., Pena, L.D., Lirer, F., 2019. Holocene hydrography evolution in the Alboran Sea: a multi-record and multi-proxy comparison. Clim. Past 15 (3), 927–942. https://doi.org/10.5194/cp-15-927-2019.

Chabaud, L., Sánchez Goñi, M.F., Desprat, S., Rossignol, L., 2014. Land–sea climatic variability in the eastern North Atlantic subtropical region over the last 14,200 years: atmospheric and oceanic processes at different timescales. Holocene 24 (7), 787–797. https://doi.org/10.1177/0959683614530439.

Cheng, H., Lawrence Edwards, R., Shen, C.-C., Polyak, V.J., Asmerom, Y., Woodhead, J., Hellstrom, J., Wang, Y., Kong, X., Spötl, C., Wang, X., Calvin Alexander, E., 2013. Improvements in 230Th dating, 230Th and 234U half-life values, and U–Th isotopic measurements by multi-collector inductively coupled plasma mass spectrometry. Earth Planet Sci. Lett. 371–372, 82–91. https://doi.org/10.1016/j.epsl.2013.04.006.

Cheng, H., Zhang, H., Spötl, C., Baker, J., Sinha, A., Li, H., Bartolomé, M., Moreno, A., Kathayat, G., Zhao, J., Dong, X., Li, Y., Ning, Y., Jia, X., Zong, B., Ait Brahim, Y., Pérez-Mejías, C., Cai, Y., Novello, V.F., et al., 2020. Timing and structure of the Younger Dryas event and its underlying climate dynamics. Proc. Natl. Acad. Sci. USA 117 (38), 23408–23417. https://doi.org/10.1073/pnas.2007869117.

Combourieu-Nebout, N., Peyron, O., Dormoy, I., Desprat, S., Beaudouin, C., Kotthoff, U., Marret, F., 2009. Rapid climatic variability in the west Mediterranean during the last 25 000 years from high resolution pollen data. Clim. Past 19.

Davis, P.T., Menounos, B., Osborn, G., 2009. Holocene and latest Pleistocene alpine glacier fluctuations: a global perspective. Quat. Sci. Rev. 28 (21–22), 2021–2033. https://doi.org/10.1016/j.quascirev.2009.05.020.

Desprat, S., Sánchez Goñi, M.F., Loutre, M.-F., 2003. Revealing climatic variability of the last three millennia in northwestern Iberia using pollen influx data. Earth Planet Sci. Lett. 213 (1–2), 63–78. https://doi.org/10.1016/S0012-821X(03)00292-9.

Dominguez-Villar, D., Fairchild, I.J., Baker, A., Wang, X., Edwards, R.L., Cheng, H., 2009. Oxygen isotope precipitation anomaly in the North Atlantic region during the 8.2 ka event. Geology 37 (12), 1095–1098. https://doi.org/10.1130/G30393A.1.

Domínguez-Villar, D., Wang, X., Krklec, K., Cheng, H., Edwards, R.L., 2017. The control of the tropical North Atlantic on Holocene millennial climate oscillations. Geology 45 (4), 303–306. https://doi.org/10.1130/G38573.1.

Fairchild, I.J., Treble, P.C., 2009. Trace elements in speleothems as recorders of environmental change. Quat. Sci. Rev. 28 (5–6), 449–468. https://doi.org/10.1016/j.quascirev.2008.11.007.

Finné, M., Woodbridge, J., Labuhn, I., Roberts, C.N., 2019. Holocene hydro-climatic variability in the Mediterranean: a synthetic multi-proxy reconstruction. Holocene 29 (5), 847–863. https://doi.org/10.1177/0959683619826634.

Fleitmann, D., Mudelsee, M., Burns, S.J., Bradley, R.S., Kramers, J., Matter, A., 2008. Evidence for a widespread climatic anomaly at around 9.2 ka before present: CLIMATIC ANOMALY AT AROUND 9.2 ka B.P. *Paleoceanography* 23 (1) n/a-n/a. https://doi.org/10.1029/2007PA001519.

Fletcher, W.J., Debret, M., Goñi, M.F.S., 2013. Mid-Holocene emergence of a low-frequency millennial oscillation in western Mediterranean climate: implications for past dynamics of the North Atlantic atmospheric westerlies. Holocene 23 (2), 153–166. https://doi.org/10.1177/0959683612460783.

Fletcher, W.J., Sánchez Goñi, M.F., Allen, J.R.M., Cheddadi, R., Combourieu-Nebout, N., Huntley, B., Lawson, I., Londeix, L., Magri, D., Margari, V., Müller, U.C., Naughton, F., Novenko, E., Roucoux, K., Tzedakis, P.C., 2010. Millennial-scale variability during the last glacial in vegetation records from Europe. Quat. Sci. Rev. 29 (21–22), 2839–2864. https://doi.org/10.1016/j.quascirev.2009.11.015.

Fohlmeister, J., 2012. A statistical approach to construct composite climate records of dated archives. Quat. Geochronol. 14, 48–56. https://doi.org/10.1016/j.quageo.2012.06.007.
Frigola, J., Moreno, A., Cacho, I., Canals, M., Sierro, F.J., Flores, J.A., Grimalt, J.O., Hodell, D.A., Curtis, J.H., 2007. Holocene climate variability in the western Mediterranean region from a deepwater sediment record: holocene climate variability. Paleoceanography 22 (2). https://doi.org/10.1029/2006PA001307.
Frisia, S., 2015. Microstratigraphic logging of calcite fabrics in speleothems as tool for palaeoclimate studies. Int. J. Speleol. 17.
García-Escárzaga, A., Gutiérrez-Zugasti, I., Marín-Arroyo, A.B., Fernandes, R., Núñez de la Fuente, S., Cuenca-Solana, D., Iriarte, E., Simões, C., Martín-Chivelet, J., González-Morales, M.R., Roberts, P., 2022. Human forager response to abrupt climate change at 8.2 ka on the Atlantic coast of Europe. Sci. Rep. 12 (1), 6481. https://doi.org/10.1038/s41598-022-10135-w.
García-Ruiz, J.M., Palacios, D., Andrés, N., López-Moreno, J.I., 2020. Neoglaciation in the Spanish Pyrenees: a multiproxy challenge. Mediterr. Geosci. Rev. 2 (1), 21–36. https://doi.org/10.1007/s42990-020-00022-9.
Gellatly, A.F., Grove, J.M., Switsur, V.R., 1992. Mid-Holocene glacial activity in the Pyrenees. Holocene 2 (3), 266–270. https://doi.org/10.1177/095968369200200309.
Genty, D., Blamart, D., Ghaleb, B., Plagnes, V., Causse, Ch, Bakalowicz, M., Zouari, K., Chkir, N., Hellstrom, J., Wainer, K., 2006. Timing and dynamics of the last deglaciation from European and North African δ13C stalagmite profiles—comparison with Chinese and South Hemisphere stalagmites. Quat. Sci. Rev. 25 (17–18), 2118–2142. https://doi.org/10.1016/j.quascirev.2006.01.030.
Gil-Romera, G., González-Sampériz, P., Lasheras-Álvarez, L., Sevilla-Callejo, M., Moreno, A., Valero-Garcés, B., López-Merino, L., Carrión, J.S., Pérez Sanz, A., Aranbarri, J., García-Prieto Fronce, E., 2014. Biomass-modulated fire dynamics during the last glacial–interglacial transition at the central Pyrenees (Spain). Palaeogeogr. Palaeoclimatol. Palaeoecol. 402, 113–124. https://doi.org/10.1016/j.palaeo.2014.03.015.
Giménez, R., Bartolomé, M., Gázquez, F., Iglesias, M., Moreno, A., 2021. Underlying climate controls in triple oxygen (16 O, 17 O, 18 O) and hydrogen (1 H, 2 H) isotopes composition of rainfall (central Pyrenees). Front. Earth Sci. 9, 633698. https://doi.org/10.3389/feart.2021.633698.
González-Sampériz, P., Aranbarri, J., Pérez-Sanz, A., Gil-Romera, G., Moreno, A., Leunda, M., Sevilla-Callejo, M., Corella, J.P., Morellón, M., Oliva, B., Valero-Garcés, B., 2017. Environmental and climate change in the southern Central Pyrenees since the Last Glacial Maximum: a view from the lake records. Catena 149, 668–688. https://doi.org/10.1016/j.catena.2016.07.041.
González-Sampériz, P., Valero-Garcés, B.L., Moreno, A., Jalut, G., García-Ruiz, J.M., Martí-Bono, C., Delgado-Huertas, A., Navas, A., Otto, T., Dedoubat, J.J., 2006. Climate variability in the Spanish Pyrenees during the last 30,000 yr revealed by the El Portalet sequence. Quat. Res. 66 (1), 38–52. https://doi.org/10.1016/j.yqres.2006.02.004.
Ilyashuk, E.A., Koinig, K.A., Heiri, O., Ilyashuk, B.P., Psenner, R., 2011. Holocene temperature variations at a high-altitude site in the Eastern Alps: a chironomid record from Schwarzsee ob Sölden, Austria. Quat. Sci. Rev. 30 (1–2), 176–191. https://doi.org/10.1016/j.quascirev.2010.10.008.
Iriarte-Chiapusso, M.J., 2016. Reviewing the Lateglacial-Holocene transition in NW Iberia: a palaeoecological approach based on the comparison between dissimilar regions. Quat. Int. 26.
Jalut, G., Dedoubat, J.J., Fontugne, M., Otto, T., 2009. Holocene circum-Mediterranean vegetation changes: climate forcing and human impact. Quat. Int. 200 (1–2), 4–18. https://doi.org/10.1016/j.quaint.2008.03.012.
Jambrina-Enríquez, M., Rico, M., Moreno, A., Leira, M., Bernárdez, P., Prego, R., Recio, C., Valero-Garcés, B.L., 2014. Timing of deglaciation and postglacial environmental dynamics in NW Iberia: the Sanabria Lake record. Quat. Sci. Rev. 94, 136–158. https://doi.org/10.1016/j.quascirev.2014.04.018.
Jiménez-Moreno, G., Rodríguez-Ramírez, A., Pérez-Asensio, J.N., Carrión, J.S., López-Sáez, J.A., Villarías-Robles, J.J., Celestino-Pérez, S., Cerrillo-Cuenca, E., León, Á., Contreras, C., 2015. Impact of late-Holocene aridification trend, climate variability and geodynamic control on the environment from a coastal area in SW Spain. Holocene 25 (4), 607–617. https://doi.org/10.1177/0959683614565955.
Kaniewski, D., Marriner, N., Morhange, C., Faivre, S., Otto, T., Van Campo, E., 2016. Solar pacing of storm surges, coastal flooding and agricultural losses in the Central Mediterranean. Sci. Rep. 6 (1), 25197. https://doi.org/10.1038/srep25197.
Kilhavn, H., Couchoud, I., Drysdale, R.N., Rossi, C., Hellstrom, J., Arnaud, F., Wong, H., 2022. The 8.2 ka event in northern Spain: timing, structure and climatic impact from a multi-proxy speleothem record. Clim. Past 18 (10), 2321–2344. https://doi.org/10.5194/cp-18-2321-2022.
Kleiven, H., Kikki, F., Kissel, C., Laj, C., Ninnemann, U.S., Richter, T.O., Cortijo, E., 2008. Reduced North Atlantic deep water coeval with the glacial lake Agassiz freshwater outburst. Science 319 (5859), 60–64. https://doi.org/10.1126/science.1148924.
Kumar, R., 2011. Neoglaciation. *Encyclopedia Of Snow, Ice And Glaciers*. Springer, USA.
Larocque-Tobler, I., Heiri, O., Wehrli, M., 2010. Late Glacial and Holocene temperature changes at Egelsee, Switzerland, reconstructed using subfossil chironomids. J. Paleolimnol. 43 (4), 649–666. https://doi.org/10.1007/s10933-009-9358-z.
Lechleitner, F.A., Day, C.C., Kost, O., Wilhelm, M., Haghipour, N., Henderson, G.M., Stoll, H.M., 2021. Stalagmite carbon isotopes suggest deglacial increase in soil respiration in western Europe driven by temperature change. Clim. Past 17 (5), 1903–1918. https://doi.org/10.5194/cp-17-1903-2021.
LeGrande, A.N., Schmidt, G.A., 2008. Ensemble, water isotope-enabled, coupled general circulation modeling insights into the 8.2 ka event: ensemble, δ^{18}O GCM of the 8.2 ka event. Paleoceanography 23 (3). https://doi.org/10.1029/2008PA001610 n/a-n/a.
Leunda, M., González-Sampériz, P., Gil-Romera, G., Aranbarri, J., Moreno, A., Oliva-Urcia, B., Sevilla-Callejo, M., Valero-Garcés, B., 2017. The Late-Glacial and Holocene Marboré Lake sequence (2612 m a.s.l., Central Pyrenees, Spain): testing high altitude sites sensitivity to millennial scale vegetation and climate variability. Global Planet. Change 157, 214–231. https://doi.org/10.1016/j.gloplacha.2017.08.008.
Leunda, M., González-Sampériz, P., Gil-Romera, G., Bartolomé, M., Belmonte-Ribas, Á., Gómez-García, D., Kaltenrieder, P., Rubiales, J.M., Schwörer, C., Tinner, W., Morales-Molino, C., Sancho, C., 2019. Ice cave reveals environmental forcing of long-term Pyrenean tree line dynamics. J. Ecol. 107 (2), 814–828. https://doi.org/10.1111/1365-2745.13077.
López-Merino, L., Silva Sánchez, N., Kaal, J., López-Sáez, J.A., Martínez Cortizas, A., 2012. Post-disturbance vegetation dynamics during the late pleistocene and the Holocene: an example from NW Iberia. Global Planet. Change 92–93, 58–70. https://doi.org/10.1016/j.gloplacha.2012.04.003.
Lorens, R.B., 1981. Sr, Cd, Mn and Co distribution coefficients in calcite as a function of calcite precipitation rate. Geochem. Cosmochim. Acta 45 (4), 553–561. https://doi.org/10.1016/0016-7037(81)90188-5.
Magny, M., Combourieu-Nebout, N., de Beaulieu, J.L., Bout-Roumazeilles, V., Colombaroli, D., Desprat, S., Francke, A., Joannin, S., Ortu, E., Peyron, O., Revel, M., Sadori, L., Siani, G., Sicre, M.A., Samartin, S., Simonneau, A., Tinner, W., Vannière, B., Wagner, B., et al., 2013. North–south palaeohydrological contrasts in the central Mediterranean during the Holocene: tentative synthesis and working hypotheses. Clim. Past 9 (5), 2043–2071. https://doi.org/10.5194/cp-9-2043-2013.
Magny, M., Vannière, B., Calo, C., Millet, L., Leroux, A., Peyron, O., Zanchetta, G., La Mantia, T., Tinner, W., 2011. Holocene hydrological changes in south-western Mediterranean as recorded by lake-level fluctuations at Lago Preola, a coastal lake in southern Sicily, Italy. Quat. Sci. Rev. 30 (19–20), 2459–2475. https://doi.org/10.1016/j.quascirev.2011.05.018.
Marcott, S.A., Shakun, J.D., Clark, P.U., Mix, A.C., 2013. A reconstruction of regional and global temperature for the past 11,300 years. Science 339 (6124), 1198–1201. https://doi.org/10.1126/science.1228026.
Martín-Chivelet, J., Muñoz-García, M.B., Edwards, R.L., Turrero, M.J., Ortega, A.I., 2011. Land surface temperature changes in Northern Iberia since 4000yrBP, based on δ13C of speleothems. Global Planet. Change 77 (1–2), 1–12. https://doi.org/10.1016/j.gloplacha.2011.02.002.
Martrat, B., Grimalt, J.O., Lopez-Martinez, C., Cacho, I., Sierro, F.J., Flores, J.A., Zahn, R., Canals, M., Curtis, J.H., Hodell, D.A., 2004. Abrupt Temperature Changes in the Western Mediterranean over the Past 250,000 Years. Science 306 (5702), 1762–1765. https://doi.org/10.1126/science.1101706.
Martrat, B., Jimenez-Amat, P., Zahn, R., Grimalt, J.O., 2014. Similarities and dissimilarities between the last two deglaciations and interglaciations in the North Atlantic region. Quat. Sci. Rev. 99, 122–134. https://doi.org/10.1016/j.quascirev.2014.06.016.
Masson-Delmotte, V., Jouzel, J., Landais, A., Stievenard, M., Johnsen, S.J., White, J.W.C., Werner, M., Sveinbjornsdottir, A., Fuhrer, K., 2005. GRIP Deuterium Excess Reveals Rapid and Orbital-Scale Changes in Greenland Moisture Origin. Science 309 (5731), 118–121. https://doi.org/10.1126/science.1108575.
Matero, I.S.O., Gregoire, L.J., Ivanovic, R.F., Tindall, J.C., Haywood, A.M., 2017. The 8.2 ka cooling event caused by Laurentide ice saddle collapse. Earth Planet Sci. Lett. 473, 205–214. https://doi.org/10.1016/j.epsl.2017.06.011.
Mauri, A., Davis, B.A.S., Collins, P.M., Kaplan, J.O., 2015. The climate of Europe during the Holocene: a gridded pollen-based reconstruction and its multi-proxy evaluation. Quat. Sci. Rev. 112, 109–127. https://doi.org/10.1016/j.quascirev.2015.01.013.
McManus, J.F., Francois, R., Gherardi, J.-M., Keigwin, L.D., Brown-Leger, S., 2004. Collapse and rapid resumption of Atlantic meridional circulation linked to deglacial climate changes. Nature 428 (6985), 834–837. https://doi.org/10.1038/nature02494.
Mesa-Fernández, J.M., Jiménez-Moreno, G., Rodrigo-Gámiz, M., García-Alix, A., Jiménez-Espejo, F.J., Martínez-Ruiz, F., Anderson, R.S., Camuera, J., Ramos-Román, M.J., 2018. Vegetation and geochemical responses to Holocene rapid climate change in the Sierra Nevada (southeastern Iberia): the Laguna Hondera record. Clim. Past 14 (11), 1687–1706. https://doi.org/10.5194/cp-14-1687-2018.
Morellón, M., Aranbarri, J., Moreno, A., González-Sampériz, P., Valero-Garcés, B.L., 2018. Early Holocene humidity patterns in the Iberian Peninsula reconstructed from lake, pollen and speleothem records. Quat. Sci. Rev. 181, 1–18. https://doi.org/10.1016/j.quascirev.2017.11.016.
Morellón, M., Valero-Garcés, B., Vegas-Vilarrúbia, T., González-Sampériz, P., Romero, Ó., Delgado-Huertas, A., Mata, P., Moreno, A., Rico, M., Corella, J.P., 2009. Lateglacial and Holocene palaeohydrology in the western Mediterranean region: the Lake Estanya record (NE Spain). Quat. Sci. Rev. 28 (25–26), 2582–2599. https://doi.org/10.1016/j.quascirev.2009.05.014.
Moreno, A., Iglesias, M., Azorin-Molina, C., Pérez-Mejías, C., Bartolomé, M., Sancho, C., Stoll, H., Cacho, I., Frigola, J., Osácar, C., Muñoz, A., Delgado-Huertas, A., Bladé, I., Vimeux, F., 2021. Measurement report: spatial variability of northern Iberian rainfall stable isotope values – investigating atmospheric controls on daily and monthly timescales. Atmos. Chem. Phys. 21 (13), 10159–10177. https://doi.org/10.5194/acp-21-10159-2021.
Moreno, A., Morellón, M., Martín-Puertas, C., Frigola, J., Canals, M., Cacho, I., Corella, J., Pérez, A., Belmonte, A., Vegas-Vilarrúbia, T., González-Sampériz, P.,

Valero-Garcés, B., 2011. Was there a common hydrological pattern in the Iberian Peninsula region during the medieval climate anomaly? PAGES News 19 (1), 16–17. https://doi.org/10.22498/pages.19.1.16.
Moreno, A., Pérez-Mejías, C., Bartolomé, M., Sancho, C., Cacho, I., Stoll, H., Delgado-Huertas, A., Hellstrom, J., Edwards, R.L., Cheng, H., 2017. New speleothem data from Molinos and Ejulve caves reveal Holocene hydrological variability in northeast Iberia. Quat. Res. 88 (2), 223–233. https://doi.org/10.1017/qua.2017.39.
Moreno, A., Stoll, H., Jiménez-Sánchez, M., Cacho, I., Valero-Garcés, B., Ito, E., Edwards, R.L., 2010. A speleothem record of glacial (25–11.6kyr BP) rapid climatic changes from northern Iberian Peninsula. Global Planet. Change 71 (3–4), 218–231. https://doi.org/10.1016/j.gloplacha.2009.10.002.
Moreno, A., Svensson, A., Brooks, S.J., Connor, S., Engels, S., Fletcher, W., Genty, D., Heiri, O., Labuhn, I., Perşoiu, A., Peyron, O., Sadori, L., Valero-Garcés, B., Wulf, S., Zanchetta, G., 2014. A compilation of Western European terrestrial records 60–8 ka BP: towards an understanding of latitudinal climatic gradients. Quat. Sci. Rev. 106, 167–185. https://doi.org/10.1016/j.quascirev.2014.06.030.
Naughton, F., Costas, S., Gomes, S.D., Desprat, S., Rodrigues, T., Sanchez Goñi, M.F., Renssen, H., Trigo, R., Bronk-Ramsey, C., Oliveira, D., Salgueiro, E., Voelker, A.H.L., Abrantes, F., 2019. Coupled ocean and atmospheric changes during Greenland stadial 1 in southwestern Europe. Quat. Sci. Rev. 212, 108–120. https://doi.org/10.1016/j.quascirev.2019.03.033.
Nielsen, L.C., De Yoreo, J.J., DePaolo, D.J., 2013. General model for calcite growth kinetics in the presence of impurity ions. Geochem. Cosmochim. Acta 115, 100–114. https://doi.org/10.1016/j.gca.2013.04.001.
O'Brien, S.R., Mayewski, P.A., Meeker, L.D., Meese, D.A., Twickler, M.S., Whitlow, S.I., 1995. Complexity of Holocene climate as reconstructed from a Greenland ice core. Science 270 (5244), 1962–1964. https://doi.org/10.1126/science.270.5244.1962.
Peck, V.L., Hall, I.R., Zahn, R., Elderfield, H., Grousset, F., Hemming, S.R., Scourse, J.D., 2006. High resolution evidence for linkages between NW European ice sheet instability and Atlantic Meridional Overturning Circulation. Earth Planet Sci. Lett. 243 (3–4), 476–488. https://doi.org/10.1016/j.epsl.2005.12.023.
Pérez-Mejías, C., Moreno, A., Sancho, C., Bartolomé, M., Stoll, H., Osácar, M.C., Cacho, I., Delgado-Huertas, A., 2018. Transference of isotopic signal from rainfall to dripwaters and farmed calcite in Mediterranean semi-arid karst. Geochem. Cosmochim. Acta 243, 66–98. https://doi.org/10.1016/j.gca.2018.09.014.
Pérez-Sanz, A., González-Sampériz, P., Moreno, A., Valero-Garcés, B., Gil-Romera, G., Rieradevall, M., Tarrats, P., Lasheras-Álvarez, L., Morellón, M., Belmonte, A., Sancho, C., Sevilla-Callejo, M., Navas, A., 2013. Holocene climate variability, vegetation dynamics and fire regime in the central Pyrenees: the Basa de la Mora sequence (NE Spain). Quat. Sci. Rev. 73, 149–169. https://doi.org/10.1016/j.quascirev.2013.05.010.
Plunkett, G., Swindles, G.T., 2008. Determining the Sun's influence on Lateglacial and Holocene climates: a focus on climate response to centennial-scale solar forcing at 2800cal.BP. Quat. Sci. Rev. 27 (1–2), 175–184. https://doi.org/10.1016/j.quascirev.2007.01.015.
Railsback, L.B., Liang, F., Vidal Romaní, J.R., Grandal-d'Anglade, A., Vaqueiro Rodríguez, M., Santos Fidalgo, L., Fernández Mosquera, D., Cheng, H., Edwards, R.L., 2011. Petrographic and isotopic evidence for Holocene long-term climate change and shorter-term environmental shifts from a stalagmite from the Serra do Courel of northwestern Spain, and implications for climatic history across Europe and the Mediterranean. Palaeogeogr. Palaeoclimatol. Palaeoecol. 305 (1–4), 172–184. https://doi.org/10.1016/j.palaeo.2011.02.030.
Rasmussen, S.O., Vinther, B.M., Clausen, H.B., Andersen, K.K., 2007. Early Holocene climate oscillations recorded in three Greenland ice cores. Quaternary Science Reviews 26 (15–16), 1907–1914. https://doi.org/10.1016/j.quascirev.2007.06.015.
Renssen, H., Seppä, H., Heiri, O., Roche, D.M., Goosse, H., Fichefet, T., 2009. The spatial and temporal complexity of the Holocene thermal maximum. Nature Geoscience 2 (6), 411–414. https://doi.org/10.1038/ngeo513.
Roberts, C.N., Woodbridge, J., Palmisano, A., Bevan, A., Fyfe, R., Shennan, S., 2019. Mediterranean landscape change during the Holocene: synthesis, comparison and regional trends in population, land cover and climate. Holocene 29 (5), 923–937. https://doi.org/10.1177/0959683619826697.
Rodrigues, T., Grimalt, J.O., Abrantes, F., Naughton, F., Flores, J.-A., 2010. The last glacial–interglacial transition (LGIT) in the western mid-latitudes of the North Atlantic: abrupt sea surface temperature change and sea level implications. Quat. Sci. Rev. 29 (15–16), 1853–1862. https://doi.org/10.1016/j.quascirev.2010.04.004.
Rossi, C., Bajo, P., Lozano, R.P., Hellstrom, J., 2018. Younger Dryas to Early Holocene paleoclimate in Cantabria (N Spain): constraints from speleothem Mg, annual fluorescence banding and stable isotope records. Quat. Sci. Rev. 192, 71–85. https://doi.org/10.1016/j.quascirev.2018.05.025.
Ruan, J., Kherbouche, F., Genty, D., Blamart, D., Cheng, H., Dewilde, F., Hachi, S., Edwards, R.L., Régnier, E., Michelot, J.-L., 2016. Evidence of a prolonged drought ca. 4200 yr BP correlated with prehistoric settlement abandonment from the Gueldaman GLD1 Cave, Northern Algeria. Clim. Past 12 (1), 1–14. https://doi.org/10.5194/cp-12-1-2016.
Sancho, C., Belmonte, Á., Bartolomé, M., Moreno, A., Leunda, M., López-Martínez, J., 2018. Middle-to-late Holocene palaeoenvironmental reconstruction from the A294 ice-cave record (Central Pyrenees, northern Spain). Earth Planet Sci. Lett. 484, 135–144. https://doi.org/10.1016/j.epsl.2017.12.027.
Scholz, D., Hoffmann, D.L., 2011. StalAge – an algorithm designed for construction of speleothem age models. Quat. Geochronol. 6 (3–4), 369–382. https://doi.org/10.1016/j.quageo.2011.02.002.
Skinner, L.C., Shackleton, N.J., 2006. Deconstructing Terminations I and II: revisiting the glacioeustatic paradigm based on deep-water temperature estimates. Quat. Sci. Rev. 25 (23–24), 3312–3321. https://doi.org/10.1016/j.quascirev.2006.07.005.
Smart, P.L., Friederich, H., 1987. Water Movement and Storage in the Unsaturated Zone of a Maturely Karstified Carbonate Aquifer. Proceedings of the conference on Environmenatl Problems in Karst Terranes and their Solutions, Dublin, Ohio, pp. 59–87.
Smith, A.C., Wynn, P.M., Barker, P.A., Leng, M.J., Noble, S.R., Tych, W., 2016. North Atlantic forcing of moisture delivery to Europe throughout the Holocene. Sci. Rep. 6 (1). https://doi.org/10.1038/srep24745.
Speranza, A., van Geel, B., van der Plicht, J., 2003. Evidence for solar forcing of climate change at ca. 850 cal BC from a Czech peat sequence. Global Planet. Change 35 (1–2), 51–65. https://doi.org/10.1016/S0921-8181(02)00091-7.
Spötl, C., 2011. Long-term performance of the Gasbench isotope ratio mass spectrometry system for the stable isotope analysis of carbonate microsamples. Rapid Commun. Mass Spectrom. 25 (11), 1683–1685. https://doi.org/10.1002/rcm.5037.
Stoll, H.M., Cacho, I., Gasson, E., Sliwinski, J., Kost, O., Moreno, A., Iglesias, M., Torner, J., Perez-Mejias, C., Haghipour, N., Cheng, H., Edwards, R.L., 2022. Rapid northern hemisphere ice sheet melting during the penultimate deglaciation. Nat. Commun. 13 (1), 3819. https://doi.org/10.1038/s41467-022-31619-3.
Stoll, H.M., Moreno, A., Mendez-Vicente, A., Gonzalez-Lemos, S., Jimenez-Sanchez, M., Dominguez-Cuesta, M.J., Edwards, R.L., Cheng, H., Wang, X., 2013. Paleoclimate and growth rates of speleothems in the northwestern Iberian Peninsula over the last two glacial cycles. Quat. Res. 80 (2), 284–290. https://doi.org/10.1016/j.yqres.2013.05.002.
Stoll, H.M., Müller, W., Prieto, M., 2012. I-STAL, a model for interpretation of Mg/Ca, Sr/Ca and Ba/Ca variations in speleothems and its forward and inverse application on seasonal to millennial scales: I-stal speleothem trace element model. G-cubed 13 (9). https://doi.org/10.1029/2012GC004183.
Swindles, G.T., Plunkett, G., Roe, H.M., 2007. A delayed climatic response to solar forcing at 2800 cal. BP: multiproxy evidence from three Irish peatlands. Holocene 17 (2), 177–182. https://doi.org/10.1177/0959683607075830.
Tan, L., Shen, C.-C., Cai, Y., Lo, L., Cheng, H., An, Z., 2014. Trace-element variations in an annually layered stalagmite as recorders of climatic changes and anthropogenic pollution in Central China. Quat. Res. 81 (2), 181–188. https://doi.org/10.1016/j.yqres.2013.12.001.
Tang, J., Köhler, S.J., Dietzel, M., 2008. Sr2+/Ca2+ and 44Ca/40Ca fractionation during inorganic calcite formation: I. Sr incorporation. Geochem. Cosmochim. Acta 72 (15), 3718–3732. https://doi.org/10.1016/j.gca.2008.05.031.
Tarrats, P., Heiri, O., Valero-Garcés, B., Cañedo-Argüelles, M., Prat, N., Rieradevall, M., González-Sampériz, P., 2018. Chironomid-inferred Holocene temperature reconstruction in Basa de la Mora Lake (Central Pyrenees). Holocene 28 (11), 1685–1696. https://doi.org/10.1177/0959683618788662.
Tesoriero, A.J., Pankow, J.F., 1996. Solid solution partitioning of Sr2+, Ba2+, and Cd2+ to calcite. Geochem. Cosmochim. Acta 60 (6), 1053–1063. https://doi.org/10.1016/0016-7037(95)00449-1.
Thatcher, D.L., Wanamaker, A.D., Denniston, R.F., Asmerom, Y., Polyak, V.J., Fullick, D., Ummenhofer, C.C., Gillikin, D.P., Haws, J.A., 2020. Hydroclimate variability from western Iberia (Portugal) during the Holocene: insights from a composite stalagmite isotope record. Holocene 30 (7), 966–981. https://doi.org/10.1177/0959683620908648.
Tremaine, D.M., Froelich, P.N., Wang, Y., 2011. Speleothem calcite farmed in situ: Modern calibration of $\delta^{18}O$ and $\delta^{13}C$ paleoclimate proxies in a continuously-monitored natural cave system. Geochimica et Cosmochimica Acta 75 (17), 4929–4950. https://doi.org/10.1016/j.gca.2011.06.005.
Usoskin, I.G., Solanki, S.K., Kovaltsov, G.A., 2007. Grand minima and maxima of solar activity: new observational constraints. Astron. Astrophys. 471 (1), 301–309. https://doi.org/10.1051/0004-6361:20077704.
Van Geel, B., Buurman, J., Waterbolk, H.T., 1996. Archaeological and palaeoecological indications of an abrupt climate change in The Netherlands, and evidence for climatological teleconnections around 2650 BP. J. Quat. Sci. 11 (6), 451–460. https://doi.org/10.1002/(SICI)1099-1417(199611/12)11:6<451::AID-JQS275>3.0.CO;2-9.
Vegas, J., Ruiz-Zapata, B., Ortiz, J.E., Galán, L., Torres, T., García-Cortés, Á., Gil-García, M.J., Pérez-González, A., Gallardo-Millán, J.L., 2010. Identification of arid phases during the last 50 cal. ka BP from the Fuentillejo maar-lacustrine record (Campo de Calatrava Volcanic Field, Spain): arid phases during the last 50 ka from the fuentillejo maar-lake record, Spain. J. Quat. Sci. 25 (7), 1051–1062. https://doi.org/10.1002/jqs.1262.
Walczak, I.W., Baldini, J.U.L., Baldini, L.M., McDermott, F., Marsden, S., Standish, C.D., Richards, D.A., Andreo, B., Slater, J., 2015. Reconstructing high-resolution climate using CT scanning of unsectioned stalagmites: a case study identifying the mid-Holocene onset of the Mediterranean climate in southern Iberia. Quat. Sci. Rev. 127, 117–128. https://doi.org/10.1016/j.quascirev.2015.06.013.
Walker, M., Head, M.J., Lowe, J., Berkelhammer, M., BjÖrck, S., Cheng, H., Cwynar, L.C., Fisher, D., Gkinis, V., Long, A., Newnham, R., Rasmussen, S.O., Weiss, H., 2019. Subdividing the Holocene Series/Epoch: Formalization of stages/ages and subseries/subepochs, and designation of GSSPs and auxiliary stratotypes. Journal of Quaternary Science 34 (3), 173–186. https://doi.org/10.1002/jqs.3097.
Wanner, H., Beer, J., Bütikofer, J., Crowley, T.J., Cubasch, U., Flückiger, J., Goosse, H., Grosjean, M., Joos, F., Kaplan, J.O., Küttel, M., Müller, S.A., Prentice, I.C.,

Solomina, O., Stocker, T.F., Tarasov, P., Wagner, M., Widmann, M., 2008. Mid- to Late Holocene climate change: an overview. Quat. Sci. Rev. 27 (19–20), 1791–1828. https://doi.org/10.1016/j.quascirev.2008.06.013.

Warken, S.F., Fohlmeister, J., Schröder-Ritzrau, A., Constantin, S., Spötl, C., Gerdes, A., Esper, J., Frank, N., Arps, J., Terente, M., Riechelmann, D.F.C., Mangini, A., Scholz, D., 2018. Reconstruction of late Holocene autumn/winter precipitation variability in SW Romania from a high-resolution speleothem trace element record. Earth Planet Sci. Lett. 499, 122–133. https://doi.org/10.1016/j.epsl.2018.07.027.

Wirth, S.B., Glur, L., Gilli, A., Anselmetti, F.S., 2013. Holocene flood frequency across the Central Alps – solar forcing and evidence for variations in North Atlantic atmospheric circulation. Quat. Sci. Rev. 80, 112–128. https://doi.org/10.1016/j.quascirev.2013.09.002.

Zielhofer, C., Fletcher, W.J., Mischke, S., De Batist, M., Campbell, J.F.E., Joannin, S., Tjallingii, R., El Hamouti, N., Junginger, A., Stele, A., Bussmann, J., Schneider, B., Lauer, T., Spitzer, K., Strupler, M., Brachert, T., Mikdad, A., 2017. Atlantic forcing of Western Mediterranean winter rain minima during the last 12,000 years. Quat. Sci. Rev. 157, 29–51. https://doi.org/10.1016/j.quascirev.2016.11.037.

Zielhofer, C., Köhler, A., Mischke, S., Benkaddour, A., Mikdad, A., Fletcher, W.J., 2019. Western Mediterranean hydro-climatic consequences of Holocene ice-rafted debris (Bond) events. Clim. Past 15 (2), 463–475. https://doi.org/10.5194/cp-15-463-2019.